FP7 2013 Cooperation Work Programme
Theme 6: Environment (Including Climate Change)

Novel indicators for identifying critical *INFRA*structure at *RISK* from Natural Hazards

Deliverable D3.3 – Uncertainty Quantification

Primary Author	Dina D'Ayala, Pierre Gehl/University College London (UCL)
WP	3
Submission Date	10/12/2015
Primary Reviewer	Pieter van Gelder, Noel van Erp\Probabilistic Solutions Consult and Training (PSCT)
Dissemination Level	PU

This project has received funding from the European Union's Seventh Programme for research, technological development and demonstration under grant agreement No 603960.

Project Information

Project Duration: 1/10/2013 - 30/09/2016

Project Coordinator:
Professor Eugene O' Brien
Roughan & O' Donovan Limited
eugene.obrien@rod.ie

Work Programme: 2013 Cooperation Theme 6:
Environment (Including Climate Change).

Call Topic: Env.2013.6.4-4 Towards Stress Testing of Critical Infrastructure Against Natural Hazards-FP7-ENV-2013-two stage.

Project Website: www.infrarisk-fp7.eu

Partners:

Roughan & O' Donovan Limited, Ireland

Eidgenössische Technische Hochschule Zürich, Switzerland.

Dragados SA, Spain.

Gavin and Doherty Geosolutions Ltd., Ireland.

Probabilistic Solutions Consult and Training BV, Netherlands.

Agencia Estatal Consejo Superior de Investigaciones Científicas, Spain.

University College London, United Kingdom.

PSJ, Netherlands.

Stiftelsen SINTEF, Norway.

Ritchey Consulting AB, Sweden.

University of Southampton (IT Innovation Centre), United Kingdom.

Document Information

Version	Date	Description	Primary Author
Rev01	15/10/2015	Deliverable D3.3 on the uncertainty quantification of single risk models	D. D'Ayala, P. Gehl
Rev02	10/12/2015	Final version for submission	D. D'Ayala, P. Gehl

Abbreviations

BN	Bayesian Network
CPT	Conditional Probability Table
DAG	Directed Acyclic Graph
FPS	Failure Path Sequence
GMPE	Ground-Motion Prediction Equation
MCS	Minimum Cut Set
MLS	Minimum Link Set
PGA	Peak Ground Acceleration
PGV	Peak Ground Velocity
SA	Spectral Acceleration
SCL	Single Connectivity Loss
SPS	Survival Path Sequence
TAZ	Traffic Analysis Zone

Executive Summary

This report conducts a quantitative analysis of the effect of various uncertainty sources on the final risk measures of a given infrastructure system, through the development of a Bayesian Network that is evaluated for different uncertainty assumptions.

First, a qualitative description of all potential uncertainty sources is proposed, through a classification between aleatory and epistemic uncertainties, at each step of the risk analysis process (i.e. hazard, physical damage and losses). This analysis is followed by a discussion on the common ways to propagate uncertainties from the input variables to the system loss measures. Bayesian Networks are identified as a relevant approach in the context of infrastructure systems, and some theoretical background is provided on how to model component failures and system performance with the Bayesian Network theory (Pearl, 1988).

Finally, the Bayesian Network method is applied to a virtual proof-of-concept example: a simple road network connection with several points of interest is considered, while being exposed to flood, ground failure and seismic hazard. The uncertainties are taken into account by the use of realistic physical models, while the effect of each assumption can be monitored at the level of the system performance indicator (i.e. single connectivity loss of the road network). Finally, it is shown that the Bayesian Network approach can be successfully applied to perform a multi-risk analysis that accounts for interactions at the fragility level.

Table of Contents

1.0 INTRODUCTION

Risk analyses are of probabilistic nature by definition, therefore uncertainty needs to be integrated into all the steps of the risk assessment process, namely the modelling of the hazard event(s), the characterisation of the exposure and the response of the vulnerable exposed infrastructure. To this end, the probabilistic hazard and fragility models that have been proposed and developed in INFRARISK deliverables D3.1 (D'Ayala et al., 2014) and D3.2 (D'Ayala et al., 2015) respectively are used to identify the various sources of uncertainty in the single risk analyses. Following the common classification between aleatory and epistemic uncertainties, it is then possible to find out which uncertainty source contributes the most to the overall variability of the loss distribution at the level of the infrastructure system. Such studies have been recently carried out in order to compare uncertainties between single risk analyses from different hazard types, as shown by Rohmer (2013) in the frame of the FP7-funded European project MATRIX (2010-2013).

While aleatory uncertainties are commonly viewed as contributing to the true randomness of the studied physical phenomenon, they are mostly considered as irreducible. Conversely, epistemic uncertainties have received more attention, since their characterisation and quantification will provide indications on which steps of the risk assessment process to focus modelling efforts, in order to obtain the greatest improvement in accuracy for the risk curve. For instance, statistical tools such as variance-based sensitivity analysis have been used by Rohmer et al. (2014) or Gehl et al. (2013) to quantify the effects of epistemic uncertainties on the seismic risk assessment of buildings. In terms of uncertainty representation, Rohmer (2013) has proposed to represent aleatory uncertainties through the shape of the risk curve (i.e. annual probability of exceedance of a given loss level), while epistemic uncertainties may be represented by confidence intervals around the median curve (see example in Figure 1).

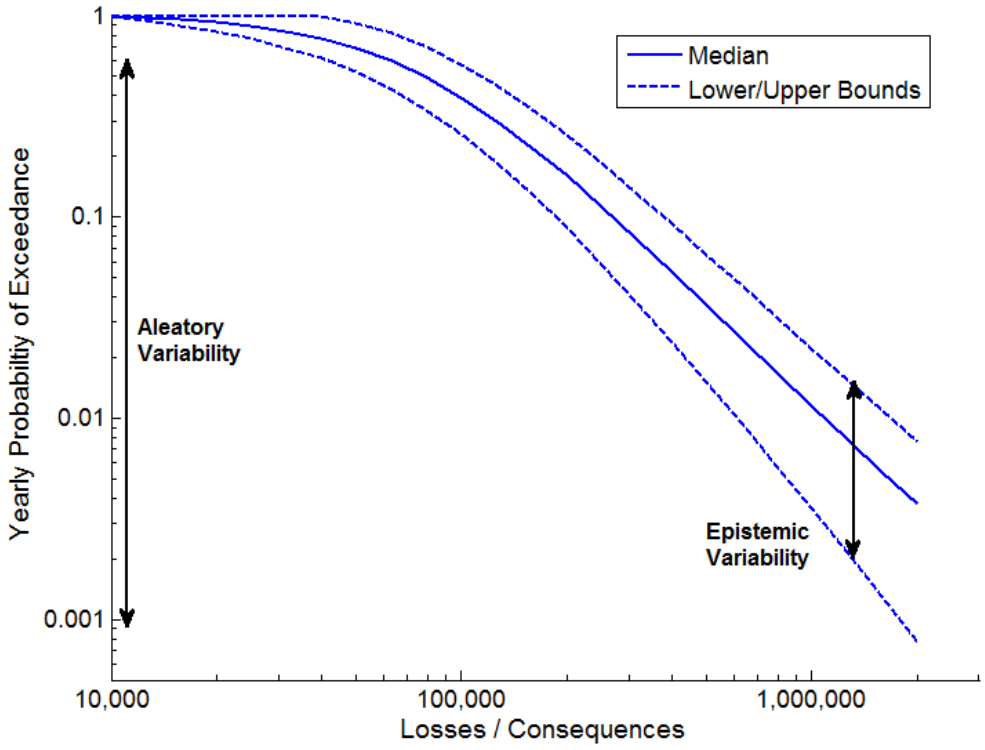

Figure 1: Representation of aleatory and epistemic uncertainties on a risk curve

A similar distinction has been introduced by Abrahamson and Bommer (2005) in the case of seismic hazard assessment; the authors claim that the inherent variability considered directly in the hazard computation (i.e. aleatory variability) leads to the shape of the hazard curve, while the epistemic uncertainty leads to alternative hazard curves. However, a caveat should be added to this distinction, since the strict Bayesians argue that all uncertainty is epistemic, in the sense that what appears as a physical property of randomness can always be viewed as an uncertain state of knowledge.

In the present report, uncertainty sources are qualitatively identified for the different hazard types considered in INFRARISK, i.e. earthquakes, landslides and floods (Section 2.1). After uncertainty propagation methods are briefly summarized, the potential of Bayesian Networks for infrastructure risk assessment is discussed and suitable Bayesian Network (BN) structures are detailed (Section 2.2).

Once the theoretical concepts have been described, they are applied to a simple hypothetical case-study, composed of a road network exposed to floods, earthquakes and earthquake-triggered landslides (Section 3). Even though the proposed case-study is virtual, input data and corresponding models are kept as realistic as possible, in order to obtain an accurate view of the effect of the difference uncertainty sources. The proposed BN structure is finally applied for different assumptions, either for single risk analyses or for a multi-risk analysis with interactions between earthquake and flood hazard at the fragility level.

2.0 THEORETICAL BACKGROUND

2.1 Sources of uncertainty in risk analyses

As part of the MATRIX project, an extensive study of uncertainties by Rohmer (2013) led to a taxonomy of uncertainty sources, as summarized in **Error! Reference source not found.**. The uncertainty sources follow the common aleatory/epistemic classification, while further distinctions are made depending on the reason for the lack of knowledge (i.e. data-, parameter-, model- or science-related).

Type of uncertainty	Main underlying causes
Aleatory uncertainty	Inherent variability (temporal and/or spatial)
Epistemic uncertainty – data	Measurement errors, representativeness of the samples, bias in the measurement process
Epistemic uncertainty – parameter	Incompleteness and imprecision of observations, experts' judgments (vagueness, conflicting views)
Epistemic uncertainty – model	Structure, several choices of "good" models
Epistemic uncertainty – scientific	Ignorance, indeterminacy, immeasurability, conflicting views

Table 1: Taxonomy of uncertainty sources, according to Rohmer (2013).

This classification is used in the following sub-sections in order to enumerate the most common uncertainty sources that should be taken into account in risk analyses.

2.1.1 Uncertainties related to hazard assessment

Different uncertainty sources may be identified based on the type of hazard considered, even though a similar structure can be observed (e.g. uncertainties due to the definition of the source event, model or parameter uncertainties in the estimation of the hazard intensities, etc.). They are summarized in **Table 2** to **Table 4**, using mainly the inventory proposed by Rohmer (2013).

Source of uncertainty	Type	Description
Estimation of design rainfall event	epistemic/data - epistemic/parameter	Design rainfall event are usually estimated through historical rainfall records, which may be subject to measurement errors or incomplete time series.
Occurrence of rainfall event	aleatory	Dependence on aleatory meteorological patterns.
Variation of river geometry over time/space	aleatory	Aleatory distribution of riverbed parameters, which may evolve with time.
Selection of models to estimate flood propagation	epistemic/model	Flow discharge may be estimated through a wide range of methods and prediction models.
Estimation of model parameters	epistemic/parameter	Physical parameters feeding the models (e.g. riverbed gradient, surface roughness, catchment area, etc.) are usually incompletely characterized.
Correlation of main channels and tributary flows	aleatory	The flow discharge at a given point may depend on the flow upstream, and on different (and usually correlated) rainfall events that may affect different tributary streams and different catchment areas.

Table 2: Main sources of uncertainty involved in the flood hazard assessment.

Source of uncertainty	Type	Description
Estimation of design earthquake event (e.g. parameters of Gutenberg-Richter law)	epistemic/data - epistemic/parameter	Design earthquake events are usually estimated through historical seismicity, which may be subject to measurement errors or incomplete time series.
Occurrence of earthquake event	aleatory	Dependence on aleatory fault rupture mechanisms.
Choice of GMPEs	epistemic/model	Seismic intensity may be predicted through a wide range of valid ground motion prediction equations.
Dispersion of GMPE (intra- and inter- event variability)	aleatory	The GMPE provides a distribution of the expected seismic intensity, whose standard deviation is a combination of intra- and inter-event variability (site-to-site and earthquake-to-earthquake variability, respectively).
Choice of truncation level for GMPE dispersion	epistemic/model	An unbounded aleatory uncertainty model for the GMPE may result in unrealistic values when low-probability high-consequence events are investigated. A truncated aleatory distribution is therefore a more common approach.
Spatial correlation between hazard intensities	aleatory	The spatial correlation of the ground motion field is built by using a correlation distance and the intra-event variability. It is an essential component of the infrastructure risk analysis.
Estimation of the site amplification factor for a specific site	epistemic/data - epistemic/parameter - epistemic/model	Amplified seismic intensities due to site effects are estimated through the study of the site of interest (e.g. soil class, measure of shear wave velocity, etc.).

Table 3: Main sources of uncertainty involved in the seismic hazard assessment.

Source of uncertainty	Type	Description
Digital Elevation Model	epistemic/data - epistemic/parameter	The quality of the DEM depends on the level of resolution and the way data has been acquired.
Failure surface depth	epistemic/model - epistemic/parameter	The depth of the failure surface is an input parameter for the hazard assessment. How this parameter is defined and used depends also on the type of model used.
Soil parameters	epistemic/parameter	Parameters such as soil unit weight, soil cohesion or angle of friction may be incompletely characterized.
Slope stability model	epistemic/model	The type of landslide model considered has an influence on the expected displacements (e.g. infinite slope mode vs circular slope failure).
Soil saturation ratio	aleatory - epistemic/data - epistemic/parameter - epistemic/model	The estimation of the soil saturation is usually a complex process which is dependent on many factors (e.g. climate, water table location, rain pattern, etc.).

Table 4: Main sources of uncertainty involved in the landslide hazard assessment.

2.1.2 Uncertainties related to damage assessment

Uncertainty sources that are involved in the estimation of physical damage may be considered as common to all hazard types, thanks to the harmonization tasks performed in INFRARISK deliverables D3.1 (D'Ayala et al., 2014) and D3.2 (D'Ayala et al., 2015), i.e. Hazard Distribution Matrix and Fragility Functions Matrix. They are summarized in **Table 5**.

Source of uncertainty	Type	Description
Characterization of the elements at risk (geometry, structural properties, etc.)	epistemic/data - epistemic/ parameter	Parameters relative to the physical assets cannot always be accurately characterized, either due to imprecise measurements or lack of census data.
Choice of fragility curves	epistemic/ model	A wide range of fragility curves may be applied to a given element, depending on the derivation method, the modelling assumptions, etc.
Dispersion of fragility curve	aleatory	The standard deviation inherent to a fragility curve represents the aleatory uncertainty that may be due to the hazard representation or the physical process leading to the failure of the element.
Choice of intensity measure	epistemic/ model	Different intensity measures may be chosen as hazard descriptors, leading to the choice of different fragility curves or hazard prediction models.
Definition of damage states	aleatory - epistemic/ model	Physical damage states are usually defined with a qualitative damage scale, while quantitative physical measures may be used to actually determine whether the element has reached the damage state or not.

Table 5: Main sources of uncertainty involved in the physical damage assessment.

2.1.3 Uncertainties related to loss assessment

Uncertainty sources that are involved in the estimation of functional losses may be considered as common to all hazard types, thanks to the harmonization tasks performed in INFRARISK deliverables D3.1 (D'Ayala et al., 2014) and D3.2 (D'Ayala et al., 2015), i.e. Hazard Distribution Matrix and Fragility Functions Matrix. They are summarized in **Table 6**.

Source of uncertainty	Type	Description
Transformation of damage states into functional losses	epistemic/model - epistemic/parameter	How the physical damage states can be translated into functional losses depends on the type of model used and on some input parameters (e.g. size/criticality of infrastructure/element).
Transformation of damage states into direct repair costs	epistemic/model - epistemic/parameter	How the physical damage states can be translated into direct repair costs depends on the type of model used and on some input parameters (e.g. size/criticality of infrastructure/element).
Transformation of damage states into repair duration	epistemic/model - epistemic/parameter	How the physical damage states can be translated into repair durations depends on the type of model used and on some input parameters (e.g. size/criticality of infrastructure/element).
Choice of system performance indicator	epistemic/model	The type of performance indicator has a significant influence on the way the system's failure or survival is perceived (e.g. connectivity-based vs capacity-based performance indicators).

Table 6: Main sources of uncertainty involved in the system loss assessment.

2.2 Use of Bayesian Networks in risk analyses

The most common approaches to propagate uncertainties in risk analyses have been previously discussed in INFRARISK deliverable D3.4 (D'Ayala and Gehl, 2015). They are summarized below:

- Monte Carlo simulations: they consist of the sampling of random realizations of the various input variables and the estimation of the final risk metric for each run. Improvements in the Monte Carlo simulation approach may be adopted in order to accelerate the convergence of the risk profile. Methods such as Importance Sampling, Latin Hypercube Sampling or Adaptive Sampling can be used to improve efficiency. Monte Carlo simulations have been used in the context of critical infrastructure exposed to seismic risk, such as the study of a system of interdependent network systems at the regional scale (Cavalieri et al., 2012) or the estimation of the road network performance in the city of Thessaloniki (Argyroudis et al., 2015).

- Logic trees with Monte Carlo simulations: they are usually used to express epistemic uncertainties that are related to model choice, since the possibility of selecting different input variables can be represented as a tree with various branches representing the different choices. Each branch is weighted (usually through expert judgment) in order to account for differences in relevance between the models. The logic tree can be used within a Monte Carlo simulation. For instance, logic trees are a common method to account for the various choices of GMPEs

that are offered to the modeller when estimating the seismic hazard intensities (Delavaud et al., 2012).

- Bayesian Event Trees: they have been introduced by Marzocchi et al. (2004, 2010) for probabilistic volcanic hazard assessment and eruption forecasting. They follow the same general principles as logic trees, except that the branches use conditional probabilities and Bayesian theory, instead of deterministic weights. This framework allows the inclusion of a priori knowledge of the event's probability, which may be updated as the evidence from the field/experiment is gathered.

One of the main issues in the probabilistic estimation of infrastructure losses lies in the high dimensionality of the problem (i.e. each individual element within the system plays a specific role with respect to the global performance), which usually leads to an intractable number of potential outcomes. This effect is even more magnified when epistemic uncertainties are included, since each realisation of a potential input variable leads to another multiplication of the space of solutions: as stated in the introduction, each realisation of a variable associated to an epistemic uncertainty source has to generate another risk curve. While Monte Carlo simulations have been shown to yield rather stable risk estimates after a reasonable number of samples (Cavalieri et al., 2012), these methods may prove to be insufficient when very low-probability and high-consequence events are investigated. In this context, it is very likely that the Monte Carlo methods will overlook such events, thus resulting in an underestimation of the risk.

Alternatively, Bayesian Networks have emerged as an adequate tool for infrastructure risk assessment and decision support (Bensi et al., 2011, 2013). Their main advantage resides in the inference process, which enables probabilities of any nodes in the BN to be updated after specifying the value or state of a given node (i.e. evidence). Bayesian inference can be worked either way, i.e. generating a forward or a backward analysis depending on whether the evidence is entered at the start or the end of the BN, respectively. Finally, exact inference algorithms such as junction trees generate the exact probability distributions for any nodes, while such quantities are usually only approximated when performing Monte Carlo simulations. This feature is an essential requirement when extreme events are considered. However, in the case of larger systems, issues due to computational loads and memory requirements start to appear, as explained in Section 2.2.3. It should be noted that the judicial use of the product and sum rules of Bayesian Probability Theory may be sufficient to perform the inference (van Erp et al., 2015), without requiring the use of Bayesian Networks and their complex junction tree algorithm. However the practical aspects of this theory and its ability to be automated for any systems remain to be demonstrated.

The application of Bayesian Networks to the field of infrastructure risk assessment has been extensively discussed and detailed in Bensi et al. (2011), however the key concepts are summarized in the following subsections.

2.2.1 General principles of Bayesian Network modelling

A BN takes the form of a *directed acyclic graph* (DAG), which is comprised of edges and nodes, which are identified as *parent* nodes or *child* nodes depending on the direction of the edges. A node without any parents is referred to as a *root node* (see example in Figure 2).

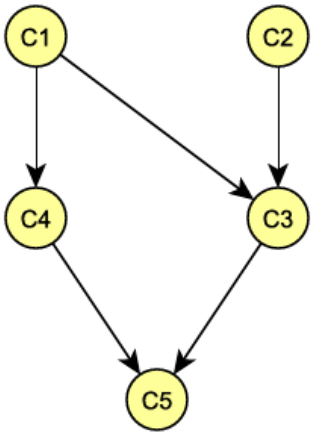

Figure 2: Example of a BN with 5 nodes (**C1** and **C2** are root nodes)

Each node represents an event that may take different states (e.g. *survival* or *failure* for a node representing an infrastructure component). The probability of each state is given by a *conditional probability table* (CPT), which represents the probabilities given the states of the parents (see **Table 7**): in the case of a root node, the CPT becomes a table of marginal probabilities (e.g. assumed probability distribution for a given input variable). It can be noticed that the CPT grows exponentially with the number of parents, which usually generates computational issues when large BN are solved.

C1	C2	C3	CPT
0	0	0	Pr(**C3**=0|**C1**=0,**C2**=0)
1	0	0	Pr(**C3**=0|**C1**=1,**C2**=0)
0	1	0	Pr(**C3**=0|**C1**=0,**C2**=1)
1	1	0	Pr(**C3**=0|**C1**=1,**C2**=1)
0	0	1	Pr(**C3**=1|**C1**=0,**C2**=0)
1	0	1	Pr(**C3**=1|**C1**=1,**C2**=0)
0	1	1	Pr(**C3**=1|**C1**=0,**C2**=1)
1	1	1	Pr(**C3**=1|**C1**=1,**C2**=1)

Table 7: Example of the CPT defining node C3, assuming binary states for C1, C2 and C3.

An inference is performed on the BN when one or more nodes are observed (i.e. *evidence* is entered by specifying a given state) and when the probabilities of the other nodes are updated. In the case of a forward analysis, evidence may be entered at the root nodes and the updated distributions can be estimated at the child nodes (e.g. distribution of infrastructure losses given the occurrence of some natural hazard events). Conversely, a backward analysis consists of the inference of the root nodes based on the observation of a given child node (e.g. updated distribution of the occurrence rate of some natural events given the observation of a given loss level).

2.2.2 The junction-tree algorithm

The junction-tree algorithm allows an exact inference to be performed on the BN, which results in exact probability distributions at the nodes of interests. The algorithm is based on the following steps (see Figure 3):

1. Moralization of the BN: all edges are represented as undirected links, and all the parents of a same node are linked by a new undirected edge, if they were not previously linked.
2. The moral graph is used to successively remove nodes until the whole graph is eliminated.
3. When a given node is removed, its adjacent nodes are connected through additional undirected edges (i.e. fill-in edges), if they were not previously linked. Then a clique is formed by the eliminated node and all its adjacent nodes.
4. Another node is eliminated, and so on… A new clique is generated only if it is not a sub-group of previous cliques.
5. Once all nodes have been eliminated, all the successive cliques form the junction tree.
6. The potential (i.e. joint probabilities) of each clique needs to be computed. Once this operation is complete, the junction tree may be used for any inference of the BN.

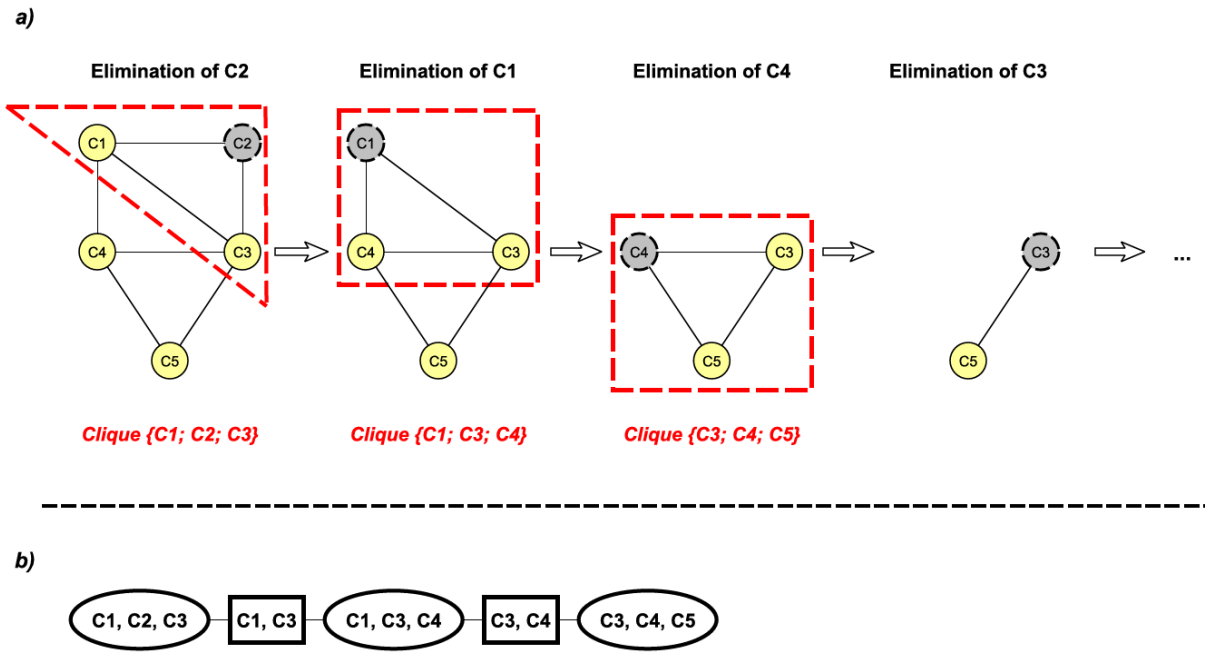

Figure 3: (a) Junction-tree algorithm applied to the BN example and (b) corresponding junction-tree containing the cliques

It appears that the elimination order in the moral graph has a major influence on the computational load of the inference, since the early or late removal of some nodes may generate non-optimal clique sizes, which may lead to an intractable number of probabilities to be evaluated. However, it has been shown that the determination of the optimal elimination order is an NP-hard problem (Wen, 1990; Franchin and Laura, 2014). In practice, BN software such as the Bayes Net toolbox (Murphy, 2007) proposes a partial optimization, where the next node that will generate either the least amount of fill-in edges or the smallest clique size is chosen. However, this method may still lead to elimination orders that lead to local optimal solutions only. Different elimination strategies have been studied by Kjaerulff (1990), depending on the topological structure of the BN.

2.2.3 Application to infrastructure systems

In the context of infrastructure systems exposed to seismic hazard, Bensi et al. (2011, 2013) have detailed the whole BN structure, from the definition of earthquake events to the computation of losses at the system level. It could be roughly decomposed into four main parts:

- Definition of the source event: i.e. magnitude range, which fault ruptures, position on the fault, etc. A simpler BN model has been proposed by Franchin (2014), where seismo-genetic sources with different activity parameters are defined, proposing a probabilistic distribution of the magnitude based on the Gutenberg-Richter law.

- Computation of the distributed seismic intensity field: based on the location of vulnerable sites (Bensi et al., 2011) or a predefined seismic grid (Franchin and Laura, 2014), the ground motion parameters are computed through GMPEs while the aleatory uncertainties are included as root nodes. Spatial correlation is accounted for by generating a correlated random field and applying it to the intra-event variability. As suggested by Bensi et al. (2011), a Dunnett-Sobel class of random variables (Dunnett and Sobel, 1955) may be used in order to approximate the correlation structure and prevent the generation of too many edges in the BN.

- Computation of the damage to infrastructure components: each node represents an infrastructure component, with the CPT being built with its respective fragility curve. Multi-state components may be implemented, even though most common examples are only based on binary elements (i.e. survival or failure).

- Computation of the system performance: a performance indicator at the system level has to be defined, usually the disconnection between two points of interest in the infrastructure system. The transition from the individual damage at component level to the global performance of the system represents one of the main challenges of infrastructure risk assessment. While some strategies have been proposed to partially solve this computational bottleneck (see paragraphs below), the issue of the high dimensionality of the solution space still hinders the application of the proposed BN approach to large systems.

Bensi et al. (2013) have investigated different strategies to facilitate the modelling of system performance, so that the computational load remains reasonable even for real-life applications. The most intuitive BN formulation is to create a converging structure where all the component nodes point to the system node: such a strategy ensures that all the information gathered from the component states can be passed on to the system level; however the size of the CPT will grow exponentially, since a system with n components with binary states will generate a CPT of 2^{n+1} elements. Therefore Bensi et al. (2013) have use the concept of minimum link sets (MLSs) and minimum cut sets (MCSs) in order to further decompose the system into chains of series and parallel sub-systems (see Figure 4):

- A MCS is a minimal set of components whose joint failure constitute failure of the system. In the case of a road network, the system symbolizing the connection between two locations could therefore be seen as an in-series assembly of parallel sub-systems (i.e. all the MCSs representing the possible cut-offs between the two points).

- A MLS is a minimal set of components whose joint survival constitutes survival of the system. In the case of a road network, the system symbolizing the connection between two locations could therefore be seen as a parallel assembly of in-series sub-systems (i.e. all the MLSs representing the possible pathways between the two points).

In Figure 4, a converging structure from the MLS nodes to the **SYS** node is adopted (naïve formulation): for a large number of MLSs, another chain structure could be built in order to sequentially assemble the MLSs to model the system performance (i.e., by definition, a system can be decomposed into a parallel assembly of MLSs).

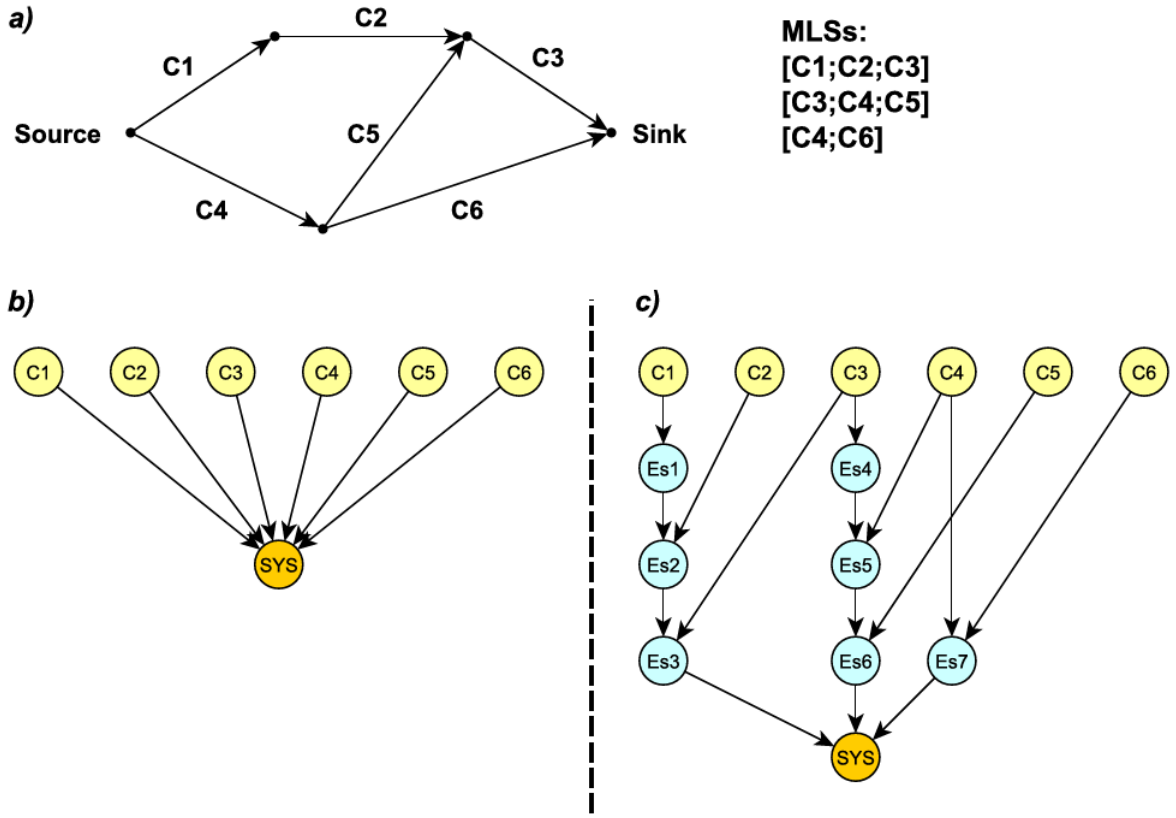

Figure 4: (a) Example of a directed network and the MLSs for the connection between one source and one sink; (b) corresponding naïve BN formulation (i.e. converging structure) and (c) BN formulation using the MLSs

Thanks to this decomposition, component nodes can form specific groups of either series or parallel sub-systems, which are easily implemented into a chain structure through intermediate nodes (i.e. survival path events $\mathbf{E_s}$ or failure path events $\mathbf{E_f}$). It is common to identify several MLSs (or MCSs) for a given infrastructure system, while some components may be involved in more than one MLS (or MCS): this may lead to a multiplication of the intermediate nodes, which may be detrimental to the computational efficiency when large systems with many MLSs or MCSs are considered. For this reason, Bensi et al. (2013) have also introduced algorithms to coalesce survival path sequences (SPSs, i.e. chain of survival events) or failure path sequences (FPSs, i.e. chain of failure events), in order to reduce the number of intermediate nodes. Additional heuristics have also been proposed in order to improve the coalescence process, either through the definition of super-components or the reduction of the possible permutations between intermediate nodes.

Even though the BN approach presents significant conceptual advantages, its applicability to large and complex infrastructure systems still remains to be demonstrated. Bensi et al. (2011) have proposed two simple examples to illustrate their developments: (i) a hypothetical road network composed of 6 bridges, where the connectivity of the regional hospital to the four cities is assessed;

(ii) the proposed California high-speed rail system to link San Francisco and Los Angeles, composed of 19 track segments (i.e. 19 vulnerable components) assembled in series.

While the MLS or MCS formulation leads to the reduction of computational loads to some extent, the following observations can be made in the case of large and complex infrastructure systems:

- The identification of the MLSs/MCSs of a given system constitutes the preliminary step before the construction of the Bayesian Network. Recursive algorithms to find all possible paths in the network may be used, however the number of possibilities increases exponentially with the size of the system. This step is crucial, since failure to identify all MLSs (resp. MCSs) will lead to an underestimation (resp. overestimation) of the system's performance.

- The large number of MLSs/MCSs for a given system usually involves infrastructure nodes in multiple MLSs/MCSs at the same time, thus leading to a number of intermediate nodes $\mathbf{E_s}/\mathbf{E_f}$ that is much larger that the number of original infrastructure nodes. Bensi et al. (2013) have addressed this issue by optimizing the layout of the chains of $\mathbf{E_s}/\mathbf{E_f}$ nodes (i.e. coalesced SPSs/FPSs), thus significantly reducing the number of intermediate nodes. However, the trade-off to this operation lies in the optimization of all possible permutations of intermediate nodes, which is also associated with an exponential computational load.

- The proposed framework has been applied to connectivity analyses only, with binary-state components. Further developments would be required if multi-state systems are considered or if the system performance indicator is a capacity measure (i.e. serviceability analysis).

3.0 SINGLE AND MULTI-RISK ANALYSES THROUGH A VIRTUAL EXAMPLE

The theoretical concepts described in the previous section are applied to a virtual proof-of-concept example, in order to demonstrate the various steps involved and to estimate which uncertainty sources are the most influential.

3.1 Characterization of the virtual proof-of-concept example

The virtual proof-of-concept example is presented in terms of asset types, network topology and potential hazards.

3.1.1 General presentation

The virtual application that has been introduced in INFRARISK deliverable D3.1 (D'Ayala et al., 2014) is reused in the context of multi-risk analyses (see basic layout in Figure 5). The aim of this exercise is to demonstrate the feasibility of the Bayesian Networks that have been detailed in the sections above, for the purpose of uncertainty treatment.

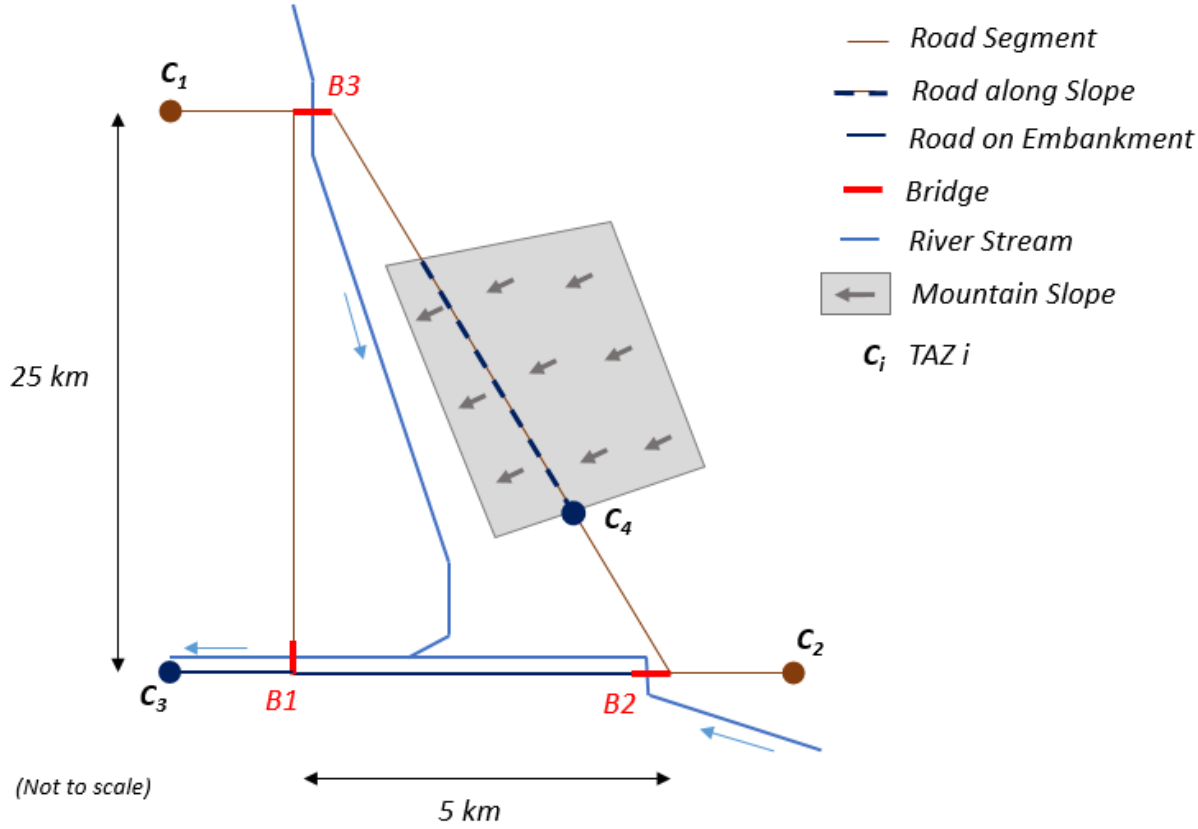

Figure 5: Layout of the proposed virtual application, with its different components

The application site is arbitrarily located somewhere around Northern Central Italy. A virtual road network is imagined, with the following components:

- Plain road segments, connecting B1 to B3 and B2 to B3;
- A road on an embankment, connecting B1 to B2 and B1 to C3;
- A road along a slope, on the B2-B3 segment;

- Three bridges (B1, B2, B3): B1 and B3 are assumed to be the same structure, with a span length of 48.8m, while B2 is assumed to be 30m long.

3.1.2 Network topology

The topology of this simplified road network may be schematized as represented in Figure 6.

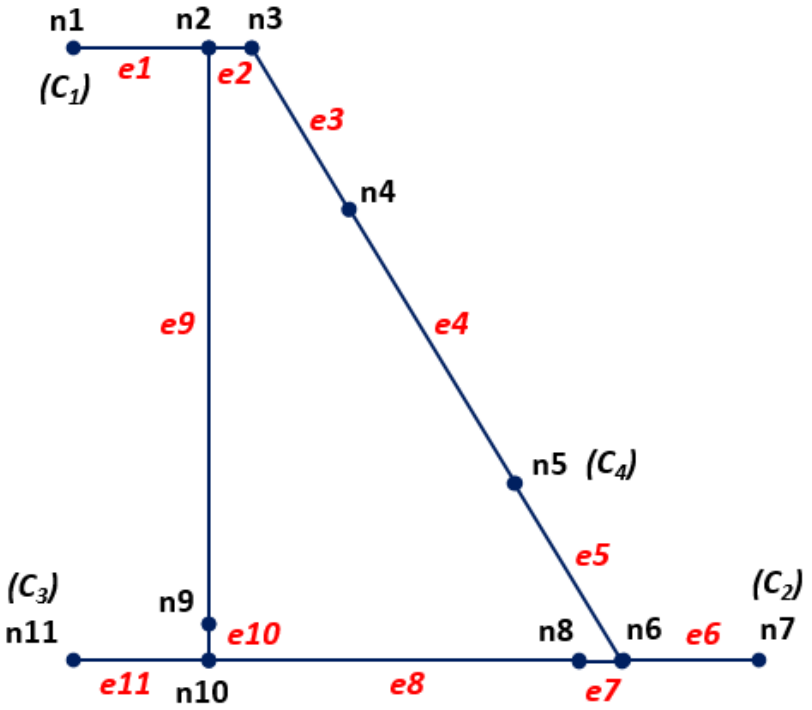

Figure 6: Topology of the proposed network

The graph and the attributes of its nodes and edges can also be represented in tabular form (see **Table 8** and **Table 9**). An undirected graph is assumed for this road network, meaning that each edge can be travelled in both directions.

Node #	*Longitude*	*Latitude*	*Description*
1	11.1794	44.2753	TAZ 1
2	11.2000	44.2753	Intersection
3	11.2006	44.2753	Intersection
4	11.2156	44.2212	Intersection
5	11.2472	44.1073	TAZ 4
6	11.2631	44.0500	Intersection
7	11.3411	44.0500	TAZ 2
8	11.2625	44.0500	Intersection
9	11.2000	44.0506	Intersection
10	11.2000	44.0500	Intersection
11	11.1836	44.0446	TAZ 3

Table 8: Description of the nodes composing the graph.

Edge #	*Start node #*	*End node #*	*Description*
1	1	2	Road segment
2	2	3	Bridge B3
3	3	4	Road segment
4	4	5	Road along slope
5	5	6	Road segment
6	6	7	Road segment
7	6	8	Bridge B2
8	8	10	Road on embankment
9	2	9	Road segment
10	9	10	Bridge B1
11	10	11	Road on embankment

Table 9: Description of the edges composing the graph.

Only the edges are considered as vulnerable in the proposed example, since the nodes may be seen as virtual objects representing the TAZs (i.e. traffic analysis zones) of the network (e.g. exits/entrances of the network, points of interest such as cities or hospitals) or the extremities of edges (i.e. intersections). Therefore the Minimum Link Sets (MLS) between each couple of TAZs are represented by enumerating the list of travelled edges only (see **Table 10**). In the present example, it is assumed that TAZs #3 and #4 are sources (i.e. origins), while TAZs #1 and #2 are potential sinks (i.e. destinations). This enables to represent the corresponding origin-destination matrix, along with the MLSs that are associated with each travel, as show in **Table 10**.

Origin / Destination	*TAZ #1*	*TAZ #2*
TAZ #3	[11;10;9;1] [11;8;7;5;4;3;2;1]	[11;8;7;6] [11;10;9;2;3;4;5;6]
TAZ #4	[4;3;2;1] [5;7;8;10;9;1]	[5;6] [4;3;2;9;10;8;7;6]

Table 10: Edge numbers composing the different MLSs for all inter-TAZ travels.

3.1.3 Hazard types and potential damage modes

The following hazard events are considered in the application:

- Earthquakes: the three bridges are assumed to be susceptible to seismic loading.
- Landslides: they are expected to happen mainly on the mountain slope, due to the occurrence of earthquakes (ground shaking) or heavy rainfall (soil saturation). Ground failure (lateral spreading) could also happen at the level of the embankment road.
- Fluvial floods due to the presence of the river streams.
- Scour at bridges due to the fluvial floods.

3.2 Modelling assumptions

Even though the proposed approach is applied to a virtual example, the underlying models and input data are selected so that they are realistic and consistent with the type of hazards and infrastructure elements that may be found in Northern Central Italy.

3.2.1 Hazard models

Hazard data and models are selected for the infrastructure area, using mainly the results from INFRARISK deliverable D3.1 (D'Ayala et al., 2014).

a. Earthquakes

The distributed seismic intensities are usually generated through ground motion prediction equations (GMPEs), which consist of empirical equations using source and site parameters such as magnitude, distance, soil class, etc. The review of existing GMPE models (Douglas, 2014) reveals a multiplication of new GMPEs over the past few years, all of them based on various assumptions and modelling approaches. This multiplicity of models may therefore be the source of epistemic uncertainties due to model choice. A common approach to include this source of epistemic uncertainty is to design a logic tree that proposes choices between various GMPEs and associated weights. Recently, Atkinson and Adams (2013) have proposed an alternative method by defining three representative GMPEs, lower, central and upper, to represent epistemic uncertainty. The three representative GMPEs are derived from available median models. Atkinson and Adams (2013) show that the three-equation model is equivalent to the use of multiple GMPEs, provided the same range of epistemic uncertainty is sampled.

These representative GMPEs are based on a set of GMPEs that are potential candidates as ground motion models for the area of interested. The central and upper/lower bound values are then obtained by a statistical treatment of the possible ground motion parameter values for various combinations of magnitude and distance. The outcome then consists of an array of discrete ground motion values over the desired range of magnitude and distance. There is no functional form associated with the model, while the epistemic uncertainty that is represented by the upper/lower bounds remains variable. Therefore Atkinson and Adams (2013) state that this representative GMPE approach has the advantage of being very flexible regarding the expression of the epistemic uncertainty and that its practical use is facilitated by the manipulation of only three possible GMPEs, as opposed to a complete logic tree.

While Atkinson and Adams (2013) have developed this approach for the generation of probabilistic seismic hazard maps for Canada, a similar representative GMPE approach has been applied to the European context with the INFRARISK project. To this end, a selection is made from recent GMPEs that are presented in the Bulletin of Earthquake Engineering Special Issue (Volume 12, issue 1, 2014) on the new generation of ground-motion models for Europe and the Middle East. Four GMPEs are chosen as the basis for the derivation of the representative GMPE model, namely, GMPEs from Akkar et al. (2014a), Bindi et al. (2014), Bora et al. (2014) and Derras et al. (2014). These GMPEs are all based on the RESORCE database of ground motion records (Akkar et al., 2014b) and they share a common validity domain (i.e. moment magnitude M_w between 4.0 and 7.6, distance between 1 and 200 km). Some of these GMPEs adopt a functional form, while others are fully data-driven through artificial neural network methods (Derras et al., 2014). For the needs of the virtual case-study, the following assumptions are used to generate the ground motions parameters:

- Normal faulting style is assumed by default;
- Epicentral distance is used as the input for the representative GMPE model. For GMPEs using others metrics such as the Joyner-Boore distance, the conversion equations proposed in Atkinson et al. (2011) are used, assuming shallow earthquakes (i.e. focal depth of 10 km).
- EC8 soil classes B are assumed, or similarly $V_{s,30}$ = 580 m/s for models that directly use shear wave velocity as a proxy to soil amplification.
- PGA is chosen as the output ground motion parameter in the present case, even though the derived representative GMPE is able to also predict PGV and SA at various periods (i.e. T = 0.05s, 0.1s, 0.2s, 0.3s, 0.5s, 1.0s and 2.0s).

The 3-equation median GMPE is plotted for a few magnitudes in Figure 7. The lower and upper bounds representing the epistemic uncertainty are estimated for the 16thand 84th percentiles (i.e. one standard deviation). Therefore the proposed model enables a complex problem to be represented by a minimum number of branches for single-site hazard analysis and mapping. Respective weights for the median, upper and lower bounds could for instance be [0.4518; 0.2741; 0.2741], according to the probability density function of the normal distribution.

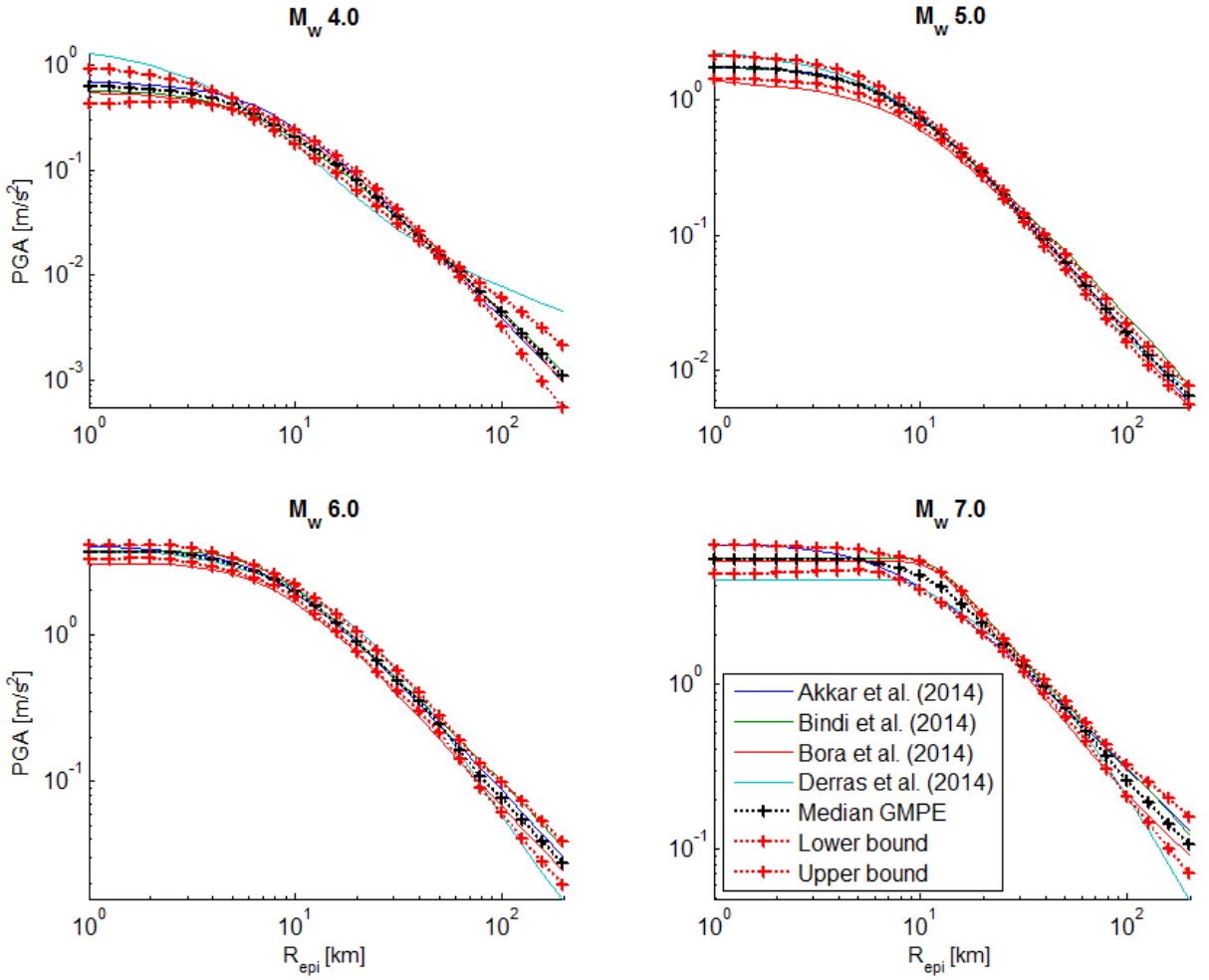

Figure 7: 3-branch representative GMPE and its underlying models

b. Floods

The rational method is used for the estimation of flow discharge at the various bridge locations, as detailed in INFRARISK deliverable D3.1 (D'Ayala et al., 2014). The flow *Q* is expressed as follows:

$$Q = \frac{C \cdot I \cdot A}{3.6} \cdot K_u \quad (1)$$

Where *C* is the run-off coefficient of the drainage area, *I* is the maximum rainfall intensity during concentration time T_c, *A* is the catchment area and K_u is the uniformity coefficient (Témez, 1991; Ferrer, 1993). The concentration time T_c may be obtained as a function of the length of the waterway between the bridge location and the catchment area, as well as the gradient of the main watercourse. The run-off coefficient is estimated through the following equation:

$$C = \frac{\left(\frac{P_d}{P_0} - 1\right) \cdot \left(\frac{P_d}{P_0} + 23\right)}{\left(\frac{P_d}{P_0} + 11\right)^2} \quad (2)$$

Where P_d is the maximum daily rainfall and P_0 is the run-off threshold, which mainly depends on the type of terrain.

Finally, the maximum rainfall intensity is obtained as a function of I_d, the design daily rainfall for an event of a given return period:

$$I = I_d \times \left[\frac{I_1}{I_d}\right]^{\frac{28^{0,10} - T_c^{\,0,10}}{28^{0,10} - 1}} \quad (3)$$

The ratio I_1/I_d represents the ratio of the hourly intensity over the average daily intensity for the given case-study area. This value is usually tabulated in guidelines or standards. The design daily rainfall is usually obtained through the analysis of rain records of weather stations over the area of interest. Sufficient time series then allow different return periods to be associated with given levels of daily rainfall.

In the present example, two catchment areas are assumed, i.e. one feeding the river branch under bridge B2 and the other linked to bridge B3. Based on the examples and assumptions used in INFRARISK deliverable D3.1 (D'Ayala et al., 2014), three return periods are proposed, as shown in **Table 11**.

Return period	***Daily rainfall***	
	Catchment area 1 (B2)	***Catchment area 2 (B3)***
50y	154 mm	235 mm
100y	174 mm	289 mm
500y	226 mm	362 mm

Table 11: Rainfall events for each return period and each catchment area.

These design rainfall events are then used to estimate the maximum flow discharge that is expected under bridges B2 and B3 (see **Table 12**), again using some of the parameters that have been assumed in INFRARISK deliverable D3.1 (D'Ayala et al., 2014).

Location	T [y]	Area [km^2]	P_d [mm]	P_d* [mm]	T_C [H]	P_0* [mm]	I_1/I_d	I_d [mm/h]	I [mm/h]	C	K_u	Q [m^3/s]
B2	50	11.96	154	146	1.04	40	9	6.1	53.5	0.33	1.07	63.22
	100	11.96	174	165	1.04	40	9	6.9	60.4	0.37	1.07	80.34
	500	11.96	226	214	1.04	40	9	8.9	78.5	0.47	1.07	129.86
B3	50	44.46	235	223	2.13	40	9	9.3	54.0	0.48	1.07	339.39
	100	44.46	289	274	2.13	40	9	11.4	66.4	0.55	1.07	481.02
	500	44.46	362	343	2.13	40	9	14.3	83.2	0.62	1.07	686.44

Table 12: Assumed parameters for rainfall events and resulting flow discharge from the rational method, for different return periods and bridge locations.

It should be noted that the bridge B1 is located at the confluence of the two river streams that cross bridge B2 and B3. For simplification purposes, it is then assumed that the maximum flow discharge at B1 is the sum of the flow discharges B2 and B3 for the various return periods. This simplistic model may still be reasonably accurate, if it can be assumed that the rainfall events over the two catchment areas are strongly correlated due to their geographical proximity (i.e. joint occurrence of maximum daily rainfall).

c. Landslides

As detailed in INFRARISK deliverable D3.1 (D'Ayala et al., 2014), an infinite slope model for superficial landslides is adopted for road segments that run along slopes. In the case of earthquake-triggered landslides, the yield acceleration k_y can be expressed as follows (Saygili, 2008; Saygili and Rathje, 2009):

$$k_y = \frac{(\mathrm{FS}-1)g}{\tan\varphi' + 1/\tan\alpha} \quad (4)$$

Where *FS* represents the factor of safety, φ' is the internal friction angle and α is the slope angle. The factor of safety under static conditions is estimated as follows:

$$\mathrm{FS} = \frac{c'}{\gamma \cdot t \cdot \sin\alpha} + \frac{\tan\varphi'}{\tan\alpha} - \frac{\gamma_w \cdot m \cdot \tan\varphi'}{\gamma \cdot \tan\alpha} \quad (5)$$

Where c' is the effective cohesion of the soil, γ is the soil unit weight, γ_w is the water unit weight and m is the saturation ratio. The soil parameters are summarized in **Table 13**: due to lack of knowledge on the shear strength of the soil, a cohesion of 0kPa and a friction angle of 40^o are assumed, as suggested by CDMG (1998). Regarding the thickness of the moving layer, Jibson et al. (2000) have stated that a typical value for superficial landslides on natural slopes is several feet, i.e. 8ft translating to 2.43m.

Parameter	*Value*
Effective cohesion (*c'*)	0 kPa
Internal friction angle (*φ'*)	40^o
Soil unit weight (*γ*)	19 kN/m^3
Failure surface thickness (*t*)	2.43 m

Table 13: Soil parameters assumed for the landslide hazard analysis.

The major difficulty lies in the estimation of the saturation ratio *m*, which potentially depends on many factors (Saygili, 2008) including; depth of the groundwater table, precipitation pattern, soil transmissivity, slope geometry, etc. It is usually estimated through detailed hydrology models or expert judgement. In the present exercise, due to the lack of relevant data, an arbitrary distribution of the saturation ratio as a function of the type of rainfall event is proposed (see **Table 14**), in order to demonstrate the impact of rainfall on the landslide hazard and to account for the uncertainties surrounding the estimation of this parameter.

Rainfall event	*Saturation ratio (m)*			
	0.20	***0.50***	***0.75***	***1.00***
none	0.8	0.2	-	-
50y	0.15	0.7	0.15	-
100y	-	0.15	0.7	0.15
500y	-	-	0.2	0.8

Table 14: Proposed distribution of the saturation ratio according to the type of rainfall event.

Therefore the proposed model allows the prediction of the occurrence of earthquake-triggered superficial landslides, by comparing the PGA value at the site with the yield acceleration k_y of the slope. Since the yield acceleration is a function of the saturation ratio, which depends on the amount of rainfall, this landslide hazard model is dependent on both the earthquake and rainfall events.

3.2.2 Fragility models

Fragility models are selected for the various infrastructure elements at risk, using mainly the results from INFRARISK deliverable D3.2 (D'Ayala et al., 2015).

a. Bridges

Bridges B1 and B3 are assumed to be identical multi-span simply-supported concrete girder bridges, as described in Nielson (2005). These bridges have been the object of a specific fragility assessment for aggregated risks (Gehl and D'Ayala, 2015a,b; D'Ayala et al., 2015). In the present context, since the measure of interest is the potential disconnection of the TAZs from the network, the failure modes that are bound to lead to the closure of the bridge are considered, namely deck unseating (failure mode 3) and collapse of substructure components (failure mode 4). The corresponding fragility model is displayed in Figure 8 (aggregation of failure modes 3 and 4).

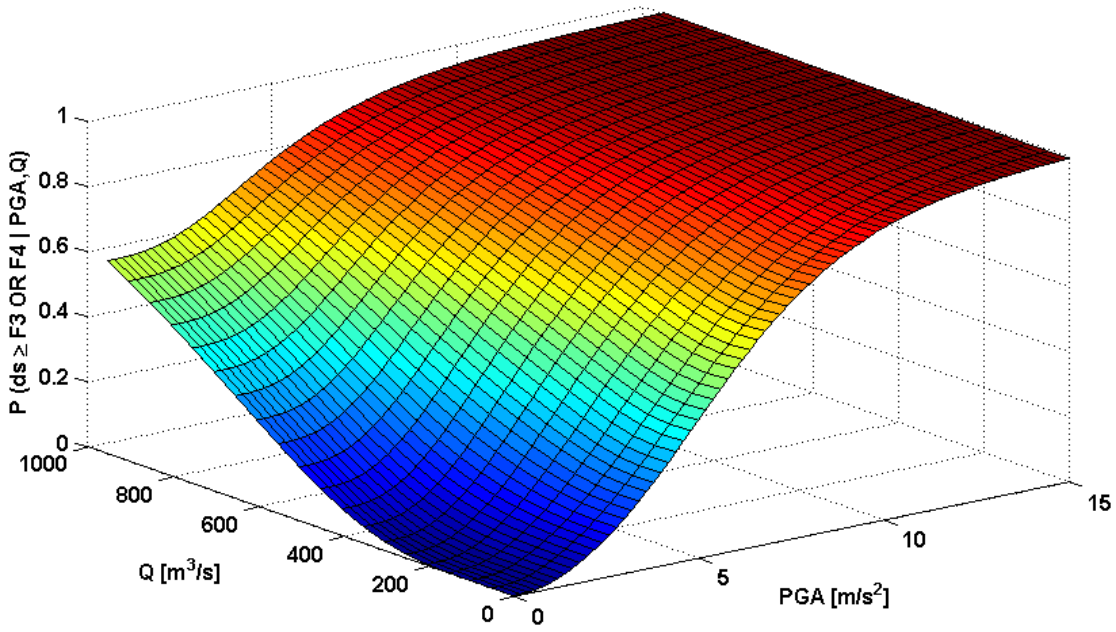

Figure 8: Fragility model for the closure of bridges B1 and B3, as a function of flow discharge *Q* and peak ground acceleration PGA

This fragility surface is able to predict the bridge failure probability due to earthquake or flood alone, as well as the interaction between flood and earthquake cumulated damages, in the case where an earthquake occurs during the period when a bridge has been damaged by a flood (i.e. submersion and scour effects). Damage due to earthquake-induced ground failure is also accounted for.

In the case of bridge B2, a smaller single-span concrete girder bridge is proposed (length of 30m), due to the reduced width of the river stream at this location. For the sake of the demonstration (i.e. use of a wide range of different models with various uncertainties), it is assumed that limited knowledge is available for this bridge type. Therefore the fragility selection procedure from the SYNER-G database (see details in INFRARISK deliverable D3.2; D'Ayala et al., 2015) is adopted here, based solely on the general taxonomy parameters of bridge B2. This method provides a median fragility curve as well as 16%-84% confidence bounds, which are meant to represent the epistemic uncertainties due to both the lack of knowledge on the bridge characteristic and the choice among various literature references. The resulting fragility model for bridge B2 is summarized in **Table 15**: only damage states DS3 and DS4 are represented, since they are the ones that are the most likely to lead to the closure of the bridge.

Damage states	***Median***		***Lower bound***		***Upper bound***	
	α **[m/s^2]**	***β***	***α*** **[m/s^2]**	***β***	***α*** **[m/s^2]**	***β***
DS3	7.458	0.832	5.007	0.268	13.298	0.851
DS4	10.389	0.906	5.035	0.265	18.532	1.163

Table 15: Fragility curves and corresponding confidence bounds for bridge B2.

It should be noted that this fragility model is only applicable to seismic risk. Since the bridge B2 is a single-span structure, the inclusion of local scour at piers is irrelevant. However, deck unseating might still occur due to the lateral hydraulic forces if the water is high enough (Kameshwar and Padgett, 2014). As a result, following the procedure presented in Gehl and D'Ayala (2015a) and D'Ayala et al. (2015), the fragility curve for the deck unseating of bridge B2 due to fluvial flood may

be represented by the following parameters: α = 2501.5m^3/s and β = 0.490. Here the mean fragility parameter α corresponds to a lower flow discharge value than for bridges B1 and B3, since the river bed is assumed to be narrower.

b. Embankments

Fragility curves for embankments exposed to earthquake-induced ground failure are selected from the study by Argyroudis and Kaynia (2015). An EC8 soil type D and an embankment height of 6m are assumed. As a result, the fragility parameters for the extensive/complete damage to these types of embankments are: α = 4.807m/s^2 and β = 0.800.

c. Road segments

Fragility curves for plain road segments exposed to earthquake-induced ground failure are also selected from Argyroudis and Kaynia (2015). Even though this study is focused on the fragility of embankments and cuts, it could be assumed that the road segments of the present case-study are built on a layer of compacted soil, which may correspond to a short embankment with stiffer soil (i.e. h = 2m and EC8 soil type C). As a result, the fragility parameters for the extensive/complete damage to these types of road segments are: α = 15.402m/s^2 and β = 1.000.

d. Roads along a slope

Fragility curves for roads running along a slope and exposed to landslides have been developed in the INFRARISK deliverable D3.2 (D'Ayala et al., 2015). They are characterized by the yield acceleration of the slope, as shown in **Table 16**. The extent of the damage is given by the amount of displacement that is induced, which is usually obtained through empirical equations such as the one by Bray and Travasarou (2007).

k_y	α [m/s^2]	β
0.05g	4.571	0.406
0.1g	7.726	0.382
0.2g	13.318	0.349
0.3g	18.418	0.328

Table 16: Fragility curves for extensive damage to urban roads along a slope, as a function of k_y (D'Ayala et al., 2015).

The proposed fragility curves can be considered as a multi-hazard fragility model, since they are expressed as a function of PGA for different values of k_y, which is linked to flood events through the soil saturation ratio *m*.

3.2.3 Functionality models

Linking physical damage states to the actual functionality losses of the various infrastructure elements represents another challenge, which has been addressed in the INFRARISK deliverable D3.2 (D'Ayala et al., 2015). Functionality loss models corresponding to global damage states of bridges have been proposed. In the present case-study, the measure of interest is the disconnection of the TAZs from the network, therefore the functionality measure that is required is whether all traffic lanes are closed or not. As a result, in the case of bridge B2, the previously developed functionality loss models are the following:

- Global damage state DS3: 50% probability of all traffic lanes being closed;
- Global damage state DS4: 100% probability of all traffic lanes being closed.

The effect of deck unseating due to fluvial flood has also to be integrated. By definition, deck unseating will lead to the closure of the bridge.

In the case of bridges B1 and B3, the specific component-based multi-risk fragility model inherently accounts for functional losses, therefore it can be concluded that the occurrence of either failure modes 3 or 4 (see Figure 8) will lead to full bridge closure.

Finally, the physical damage states that have been considered for plain road segments, embankments and roads along slopes (i.e. extensive/complete damage) are found to automatically lead to the closure of all traffic lanes, according to the expert-based survey that has been conducted in INFRARISK deliverable D3.2 (D'Ayala et al., 2015).

3.2.4 System performance indicator

The current developments in the use of Bayesian Networks for the risk analysis of infrastructure systems only permit the prediction of connectivity-based performance indicators, since estimating capacity-based indicators (e.g. through traffic analysis models) would require a much deeper analysis of the physical network and generate intractable computations. Therefore the Single Connectivity Loss (SCL) index is chosen in order to represent the amount of disconnected TAZs (i.e. locations that cannot be reached anymore by the road). The SCL index has been introduced by Poljanšek et al. (2012) and has been previously used within the SYNER-G project (2009-2013):

$$SCL = 1 - \left\langle \frac{N_s^i}{N_0^i} \right\rangle_{i \in [1..n]} \quad \textbf{(6)}$$

Where <> is the averaging operation over the *n* sinks of the system, N_0^i is the number of sources for sink *i* in normal conditions and N_s^i is the number of remaining sources for sink *i* in post-disaster conditions. In the present case-study, two sinks, TAZs #1 and #2, are potentially connected to two sources, TAZs #3 and #4:

$$SCL = 1 - \frac{1}{2} \cdot \left[\frac{N_s^1}{2} + \frac{N_s^2}{2} \right] \quad \textbf{(7)}$$

The objective of the following analysis is therefore to estimate how many sources N_s^1 and N_s^2 remain connected to the sinks. This is done by evaluating whether the various MLSs that have previously identified are still viable. Finally, it should be noted, that in this reduced example, the SCL index may only take a reduced set of possible values: 0, 0.25, 0.50, 0.75 and 1.

3.3 Summary of uncertainty sources

The models and assumptions used in the present examples include the following sources of uncertainty, based on the general uncertainty framework described in Section 2.1:

- **Aleatory uncertainties:**
    - Inter-event variability of the GMPE model: it is represented by the normally distributed term η that is associated with each GMPE.
    - Intra-event variability of the GMPE model: it is specific to each site i and is represented by the normally distributed term ε_i. A spatial correlation structure is adopted between the vulnerable sites to generate the terms ε_i, based on a correlation distance.
    - Dispersion inherent to the fragility models: it corresponds the standard-deviation of the fragility functions. It does necessarily include aleatory uncertainties, since it is usually a combination of record-to-record variability, modelling assumptions and definition of the damage state.
- **Epistemic uncertainties:**
    - Choice of a GMPE: the 3-branch representative GMPE that has been discussed above is used here in order to represent the epistemic uncertainties due to model choice.
    - Choice of a fragility curve: for bridge B2, only global features are identified (e.g. deck type, spans, pier type, etc.) and a hybrid fragility model is derived from existing references, along with confidence bounds.
    - Dispersion inherent to the functionality modes: for bridge B2, a probabilistic functionality loss model is adopted given the physical damage states, since closure of the bridge may not be accurately predicted due to the lack of knowledge (i.e. meaning of the damage states considered).
    - Estimation of the yield acceleration k_y: the evolution of the soil saturation ratio, which is used in the computation of the yield acceleration, along with the rainfall pattern, is completely assumed due the absence of any predictive model and relevant expertise on this aspect.
    - Interactions between the different risks: the interaction between the flood and the seismic hazard is represented by the development of a multi-risk fragility model for bridges B1 and B3. This model is based on the assumption that a given bridge might still be damaged after a flood event, thus increasing its vulnerability from a subsequent earthquake: therefore a time frame is needed in order to account for this risk interaction (i.e. duration during which the bridge might remain unrepaired).

3.4 Corresponding Bayesian Network

Based on the previously discussed assumptions, a Bayesian Network (BN) can be built in order to perform the multi-risk analysis of the road network (see Figure 9): all the successive steps of the risk analysis are present, i.e. the definition of the source events, the hazard events, the physical damage events and the functional consequences at the system level.

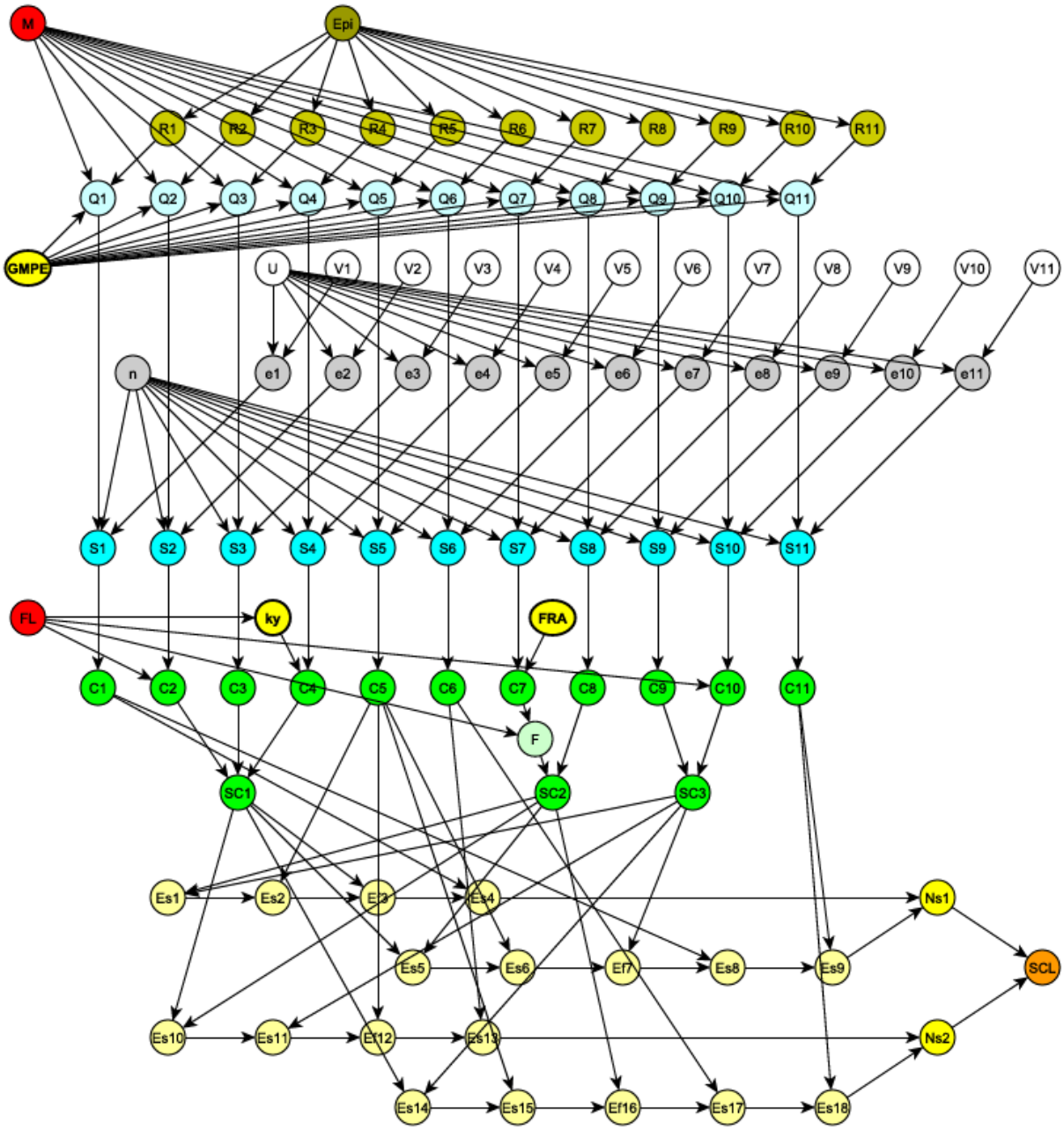

Figure 9: Bayesian Network used for the multi-risk analysis of the infrastructure system

The different nodes involved in the BN are the following:

- **M**: magnitude range of the possible earthquake events. An extra state has been added in order to account for no earthquake occurring.
- **Epi**: discretized locations of the epicentre of the earthquake events.
- **R_i**: epicentral distance from the infrastructure elements.
- **GMPE:** possible GMPEs to be used in the analysis (model uncertainty).
- **Q_i:** median PGA values at the sites of interest, without any uncertainty factors.
- **U** and **V_i**: nodes containing the standard normal distribution in order to represent the spatial correlation of the seismic hazard at the 11 vulnerable sites.

- **e_i:** intra-event uncertainty term, specific to each element, due to the spatial correlation assumption.
- **n:** inter-event uncertainty term, common to all elements.
- **S_i:** final PGA values at the sites of interest, including intra- and inter-event uncertainties.
- **FL:** range of rainfall events for the three return periods, being directly linked to the flow discharge value at each bridge location. An extra state has been added in order to account for no flood occurring.
- **k_y:** possible values of yield acceleration based on the type of rainfall event.
- **FRA:** possible fragility curves for bridge B2 to be used in the analysis (i.e. median curve and confidence bounds).
- **C_i:** damage states of the infrastructure elements.
- **F:** functional states of bridge B2, depending on the seismic physical damage states and on the flow discharge value.
- **SC_1:** super-components, i.e. groups of elements that are found to be in-series within the MLSs.
- **Es_i:** survival events for the elements within the same MLS.
- **Ef_i:** failure events for the elements for different MLSs.
- **Ns_i**: number of sources still connected to sink *i*.
- **SCL**: single connectivity loss.

In Figure 9, the red nodes represent the input to the Bayesian Networks in terms of potential source events (i.e. earthquakes and rainfall). The blue nodes represent the computation of the distributed hazard values, based on the geographical coordinates of the system (brown nodes). The green nodes represent the damages and functional losses to infrastructure elements, while the yellow nodes represent the computation of the disconnected TAZs and the SCL based on the failures of elements. Finally, the grey nodes represent aleatory uncertainty sources (i.e. intra- and inter-event variability), while the highlighted bright yellow nodes represent epistemic uncertainty source (i.e. model choice and parameter assumptions).

Regarding the system functionality part of the BN, each source-sink couple has to be assessed separately with its respective MLSs. If the efficient MLS formulation with distinct survival path sequences (SPSs) from Bensi et al. (2013) were used, the bottom of the BN would look like in Figure 10. In this figure, only the BN structure to estimate whether TAZs #3 and #1 are disconnected is presented: it is composed of MLSs [1;9;10;11] and [1;2;3;4;5;7;8;11], as previously detailed (see **Table 10**). The **Es_i** nodes represent survival events for in-series systems and their CPT takes the form of a Boolean table, as shown in **Table 17**. Conversely, the **SYS** node corresponds to a parallel assembly, since it takes all MLSs to fail in order for the disconnection to occur.

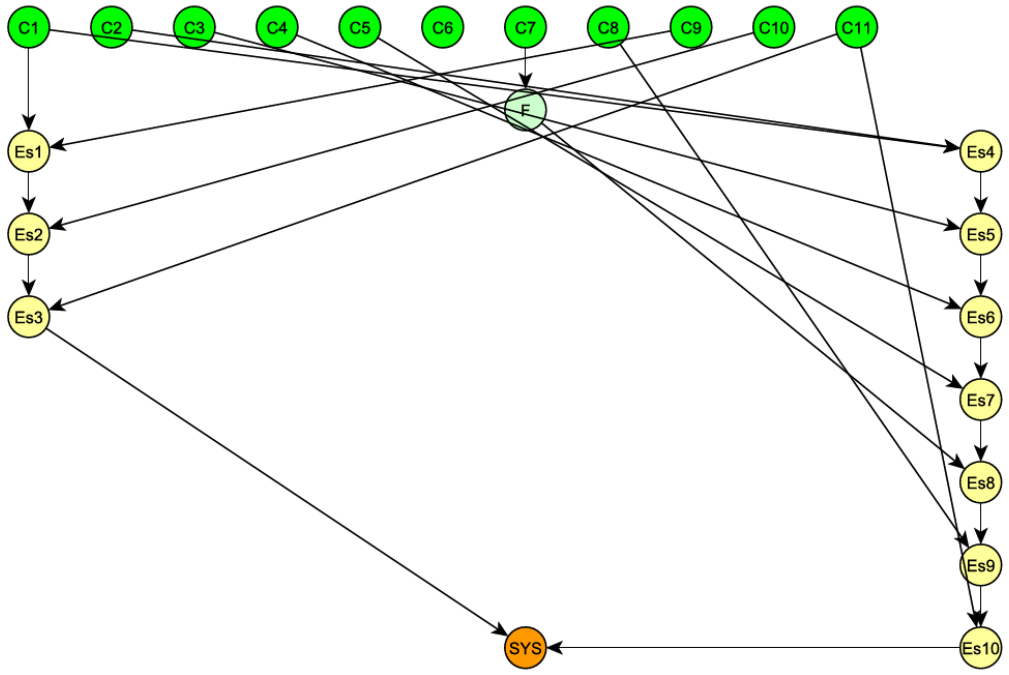

Figure 10: Efficient MLS formulation with distinct SPSs, in order to evaluate the disconnection of TAZ #3 with TAZ #1 (with two MLSs)

Binary states			Probabilities
C_i	Es_{i-1} / C_{i-1}	Es_i	Series system
0	0	0	1
1	0	0	0
0	1	0	0
1	1	0	0
0	0	1	0
1	0	1	1
0	1	1	1
1	1	1	1

Table 17: Conditional probability table for Es_i nodes, with binary states. The convention is 0 for survival (i.e. damage state 0) and 1 for failure (i.e. damage state 1).

As stated by Bensi et al. (2013), some of the **Es_i** nodes present in Figure 10 are redundant since they are present for the same component event: for large systems, this issue could lead to unnecessary large BNs that would become too complex to solve. Therefore it is necessary to simplify this BN structure: a first strategy could be to reduce all in-series components that are common to the different MLSs. An analysis of shows that sets of components [2;3;4], [7;8] and [9;10] can be aggregated into super-components #1, #2 and #3 (see Figure 11).

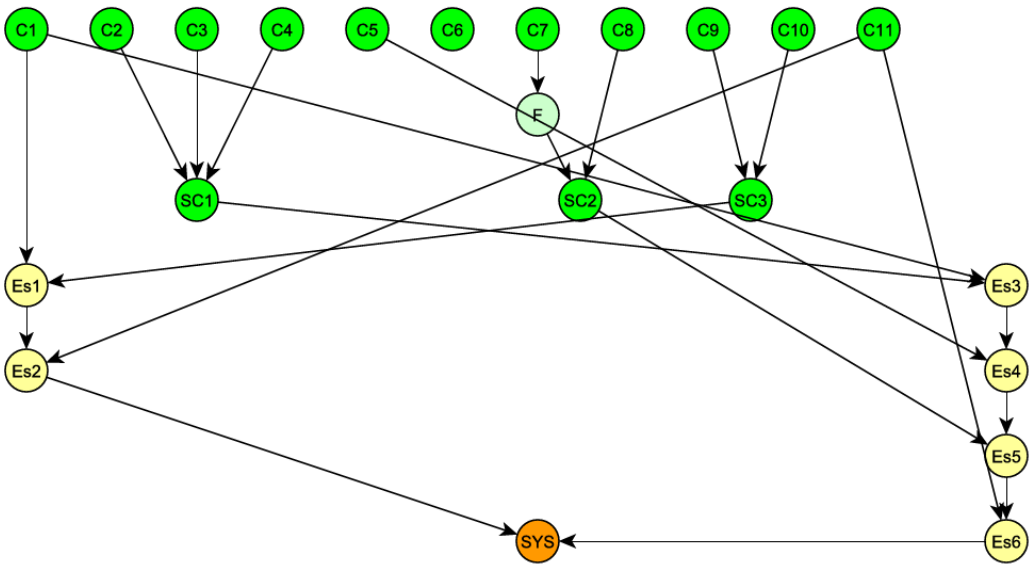

Figure 11: Efficient MLS formulation with distinct SPSs and super-components, in order to evaluate the disconnection of TAZ #3 with TAZ #1 (with two MLSs)

Once the super-components have been introduced, it appears that the **Es** nodes corresponding to components $\mathbf{C_1}$ and $\mathbf{C_{11}}$ are redundant, since they are used in both MLSs. They could therefore be moved to the end of a chain structure leading to **SYS** (i.e. they could be seen as a bottleneck). Besides these two nodes, the **Es** nodes corresponding to $\mathbf{C_5}$, $\mathbf{SC_1}$ and $\mathbf{SC_2}$ components remain in the second MLS, and they can be moved to the beginning of the chain structure as a series system. Finally, there is only one node left in the first MLS, i.e. the **Es** node relating to $\mathbf{C_5}$ component. This node can be added to the chain structure, however it must bear the information that it belongs to a different MLS, thus resulting in a parallel assembly with the nodes from the other MLS. Therefore the **Es** node has to be turned in an **Ef** node, or failure event node, as introduced by Bensi et al. (2013). The CPT of such a node is detailed in **Table 18**. The final BN that predicts the disconnection between TAZs #3 and #1 is presented in Figure 12.

Binary states			**Probabilities**
$\mathbf{C_i}$	$\mathbf{Es_{i-1}}$ / $\mathbf{C_{i-1}}$	$\mathbf{In_i}$	**Parallel system**
0	0	0	1
1	0	0	1
0	1	0	1
1	1	0	0
0	0	1	0
1	0	1	0
0	1	1	0
1	1	1	1

Table 18: Conditional probability table for Ef_i nodes, with binary states. The convention is 0 for survival (i.e. damage state 0) and 1 for failure (i.e. damage state 1).

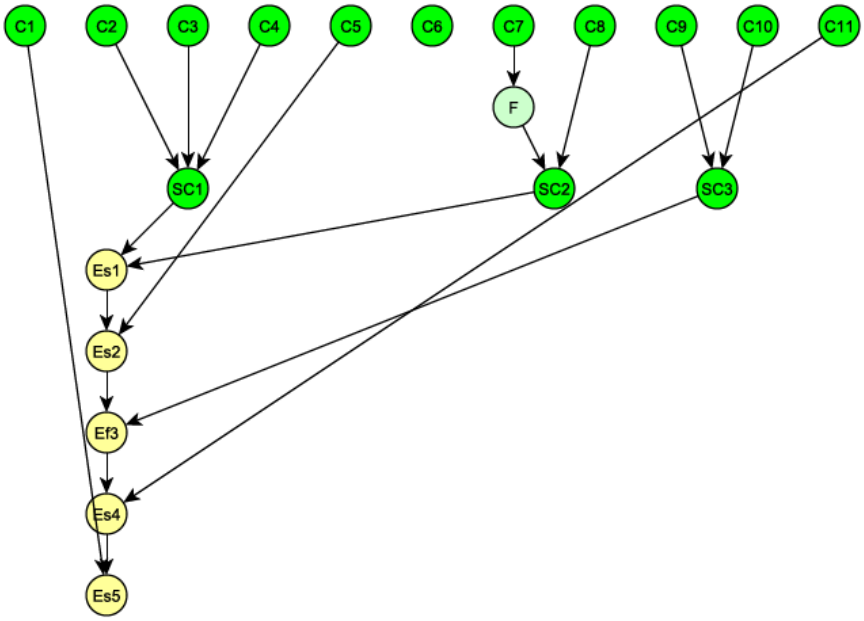

Figure 12: Efficient MLS formulation with coalesced SPSs in a chain structure and super-components, in order to evaluate the disconnection of TAZ #3 with TAZ #1 (with two MLSs)

The comparison between Figure 10 and Figure 12 shows the reduction in the number of BN nodes that is induced by the aggregation of SPSs into a chain structure and the use of super-components. This effect is even more visible at the scale of the whole system, since previously defined super-components may be reused for all MLSs. In the present example, the whole BN with an efficient MLS formulation and distinct SPSs would result in 118 nodes, while it has been reduced to 99 nodes by coalescing the SPSs (see Figure 9).

Finally, the BN can be implemented into the Bayes Net toolbox (Murphy, 2007), where a junction-tree algorithm is used in order to perform the Bayesian inference and predict the probabilistic distribution of SCL based on the occurrence rate of the source events (i.e. earthquake and rainfall).

3.5 Multi-risk analysis

Currently, there are limited examples in the literature of multi-risk analyses that account for all possible interactions, from the source events to the loss estimations. Selva (2013) relies on a formal statistical model to include multi-risk interactions at hazard, vulnerability and exposure levels. This approach is applied to two hypothetical cases, i.e. (i) seismic risk and volcanic ash deposits and (ii) tsunami risk induced by damaging earthquakes. Mignan et al. (2014) have simulated time series that may include any number of source events or triggered events, depending on their rate of occurrence. These time-dependent scenarios are randomly generated through a sequential Monte Carlo method that is able to treat either independent coinciding events or triggered/cascading events. This approach is applied to a virtual city that is potentially exposed to a wide range of hazard types (i.e. the “MATRIX Virtual City” concept). The results are presented under the form of a risk matrix (i.e. loss vs frequency) and the risk migration between different interaction assumptions can be observed.

Since the BN approach proposed in the present report may not be easily applicable to a time-dependent framework with sequential events, it is first checked whether the BN can comply with the

multi-risk probabilistic model that has been introduced by Selva (2013). He introduces the concept of a persistence time window ΔT_p, which is crucial to properly model the effect of a second hazard event while the effects of the first event in terms of vulnerability and exposure are still present. Considering two potential events E1 and E2, the probability of E1 occurring while the effects of E2 are still present is given by the following expression (Selva, 2013):

$$H^{(E1,E2)}\left(x_j\right) = H^{(E1|E2)}\left(x_j;\Delta T_p\right)\cdot \Pr\left(E2;\Delta T\right) \quad \textbf{(8)}$$

Where $H^{(.)}(x_j)$ represents the probability of having a given hazard event with the value $x \geq x_j$, and ΔT is the global exposure time over which the risk is estimated. In the context of the present case-study example, E2 represents the rainfall event, E1 the earthquake event and the exposure time is set as ΔT = 1 year; this corresponds to the INFRARISK objective of quantifying the yearly losses for the road infrastructure. Finally, it is assumed that the persistence time window ΔT_p could be around 1 month (i.e. accounting for the time needed by the flood to recede and the duration of the subsequent repair operations).

Moving to the risk factor $R_c(\geq l)$, which gives the probability of exceeding losses l over time period ΔT, Selva (2013) defines the following expression for the risk due to E1 with possible interactions with E2:

$$R_c^{(E1)}\left(\geq l\right) = R_c^{(E1,E2)}\left(\geq l\right) + R_c^{(E1,\overline{E2})}\left(\geq l\right) \quad \textbf{(9)}$$

Where the first term on the right side is referred to as the *co-active risk* factor: it represents the part of the risk that is only generated by the joint occurrence of E1 and E2 in the same time window ΔT_p. The second term is the *isolated risk* factor, which can be seen as the part of risk that remains when E1 is not interacting with E2. It can be further decomposed into two distinct parts:

$$R_c^{(E1,\overline{E2})}\left(\geq l\right) = R_c^{(E1,s)}\left(\geq l\right) - R_c^{(E1,v)}\left(\geq l\right) \quad \textbf{(10)}$$

The first term is referred to as the *single risk* factor for E1, since it represents the risk due of E1 over the whole ΔT period, without considering the effects of E2. The second term is referred to as the *virtual risk* factor, since it represents the risk due to both E1 and E2 over ΔT, except that the fragility and exposure models are not updated due to the potential impacts of E2.

This framework is then applied to the BN approach proposed here. The modularity of the BN and its ability to handle different types of evidence (i.e. assumptions or observations) permits the generation of risk curves for the different assumptions above:

- **Earthquake risk only (*single risk*):** the FL node (flood intensity) is evidenced with Pr(FL=0) = 1, while the probability of occurrence of the M node is set for ΔT = 1 year.
- **Flood risk only (*single risk*):** the M node (magnitude range) is evidenced with Pr(M=0) = 1, while the probability of occurrence of the FL node is set for ΔT = 1 year.
- **Interacting earthquake and flood risks (*co-active risk*):** the full distributions of FL and M nodes are sampled. The probability of occurrence of FL is set for ΔT = 1 year, while ΔT_p = 1 month is used for M.

- **Interacting earthquake and flood risks without updating fragility model (*virtual risk*):** it is obtained by summing the *flood single risk* (with ΔT = 1 year) and the *earthquake single risk* (with ΔT_p = 1 month).
- **Earthquake risk outside the time window of flood risk (*isolated risk*):** it is obtained by subtracting the *virtual risk* from the sum of the flood and earthquake *single risks* (both with ΔT = 1 year).
- **Global risk from both earthquake and rainfall events over a year (*multi-risk*):** it is obtained by summing the *isolated risk* factor and the *co-active risk* factor.

The BN can then be solved for these different scenarios, and the resulting risk curves (i.e. year probability of exceedance for the different SCL values) are presented in Figure 13 and **Table 19**.

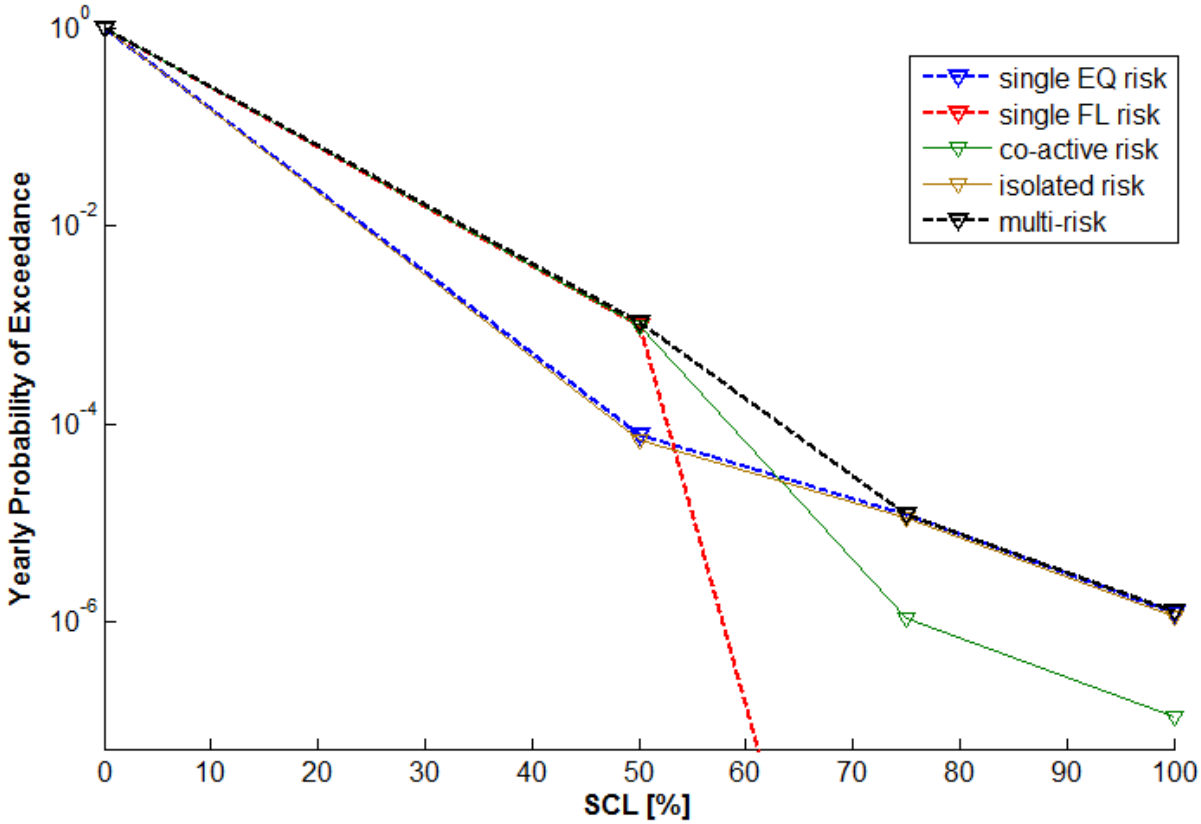

Figure 13: Risk curves for the SCL index, using the different risk factors

SCL	Risk factor					
	Single EQ	Single FL	Co-active	Virtual	Isolated	Multi
50%	7.5916E-05	9.8785E-04	9.9449E-04	9.9421E-04	6.9560E-05	***1.0641E-03***
75%	1.2272E-05	2.5635E-13	1.0977E-06	1.0274E-06	1.1244E-05	***1.2342E-05***
100%	1.2498E-06	NaN	1.1082E-07	1.0463E-07	1.1452E-06	***1.2560E-06***

Table 19: Yearly probability of exceeding the given SCL value with the different risk factors considered.

Selva (2013) has also introduced δR, a single risk bias measure which estimates the bias in the risk measure when only single risk analyses are performed, without accounting for the interaction effects:

$$\delta R = R_c^{(E1,E2)} - R_c^{(E1,v)} \quad (11)$$

It consists in the difference between the virtual risk factor and the co-active risk factor. Selva (2013) also proposes to normalize this bias measure by the *single risk* factor. However, in the present case-study, both hazard events have damaging potential and E2 (i.e. rainfall event) is not limited to the role of an aggravating risk factor. Therefore it is proposed here to normalize by the sum of both *single risk* factors:

$$\delta R_{\%} = \frac{R_c^{(E1,E2)} - R_c^{(E1,v)}}{R_c^{(E1)} + R_c^{(E2)}} \quad (12)$$

The multi-risk bias values for the present example are detailed in Table 20. The effect of multi-risk interaction looks rather light, i.e. the bias measure not exceeding 1% with ΔT_p = 1 month, however it is interesting to observe that the bias follows the same trend as the risk migration estimated by Mignan et al. (2014): when considering multi-risk interactions, extreme consequence events tend to have a large rate of occurrence (i.e. SCL = 75% and SCL = 100% in the present case), which seems to have partly migrated from the rate of occurrence of less severe events (e.g. SCL = 50%). The risk bias measure is also presented for different values of the persistence time window ΔT_p, thus showing the significant influence of the temporal aspect on multi-risk analyses.

SCL	$\delta R_{\%}$ with ΔT_p = 1 month	$\delta R_{\%}$ with ΔT_p = 1 week	$\delta R_{\%}$ with ΔT_p = 3 months
50%	**0.027%**	**0.006%**	**0.080%**
75%	**0.574%**	**0.132%**	**1.719%**
100%	**0.495%**	**0.114%**	**1.483%**

Table 20: Relative risk bias measure using SCL as the system's loss measure.

3.6 Sensitivity from uncertainty sources

This section details the effects of some of the uncertainties sources that have been identified. Such a task can be efficiently conducted by taking advantage of the BN approach, which enables the value of some nodes to be forced (i.e. evidence input) and the distribution of the outputs through an exact inference can be observed.

The aforementioned computations have been conducted by bounding the aleatory uncertainties of the GMPE to the +/- 1 $\sigma_{a,tot}$ interval, where $\sigma_{a,tot}$ is the standard deviation that results from the composition of intra- and inter-event variability (which are inherent to the GMPE model):

$$\sigma_{a,tot} = \sqrt{\sigma_{intra}^2 + \sigma_{inter}^2} \quad (13)$$

The effect of the range of the possible uncertainty values is illustrated in Figure 14. As expected, the inclusion of aleatory uncertainties in the hazard prediction models results in a significant increase of the expected losses. It is interesting to note that the loss probabilities tend to converge and even slightly decrease for +/- 3 $\sigma_{a,tot}$. For such a level of variability, very high and unrealistic hazard intensity values are sampled, which may lead to a saturation of the fragility function s (i.e. failure probabilities equal to 1), while in the meantime, very low hazard intensities are also sampled, thus resulting in no failure at all. Truncating the ground motion variability at +/- 1 $\sigma_{a,tot}$ appears to constitute a sound assumption in the present case: the highest generated values with this sigma

level are of the order of 20~25 m/s, while the use of +/- 2 $\sigma_{a,tot}$ or above would lead to intensity values that are not physically realistic.

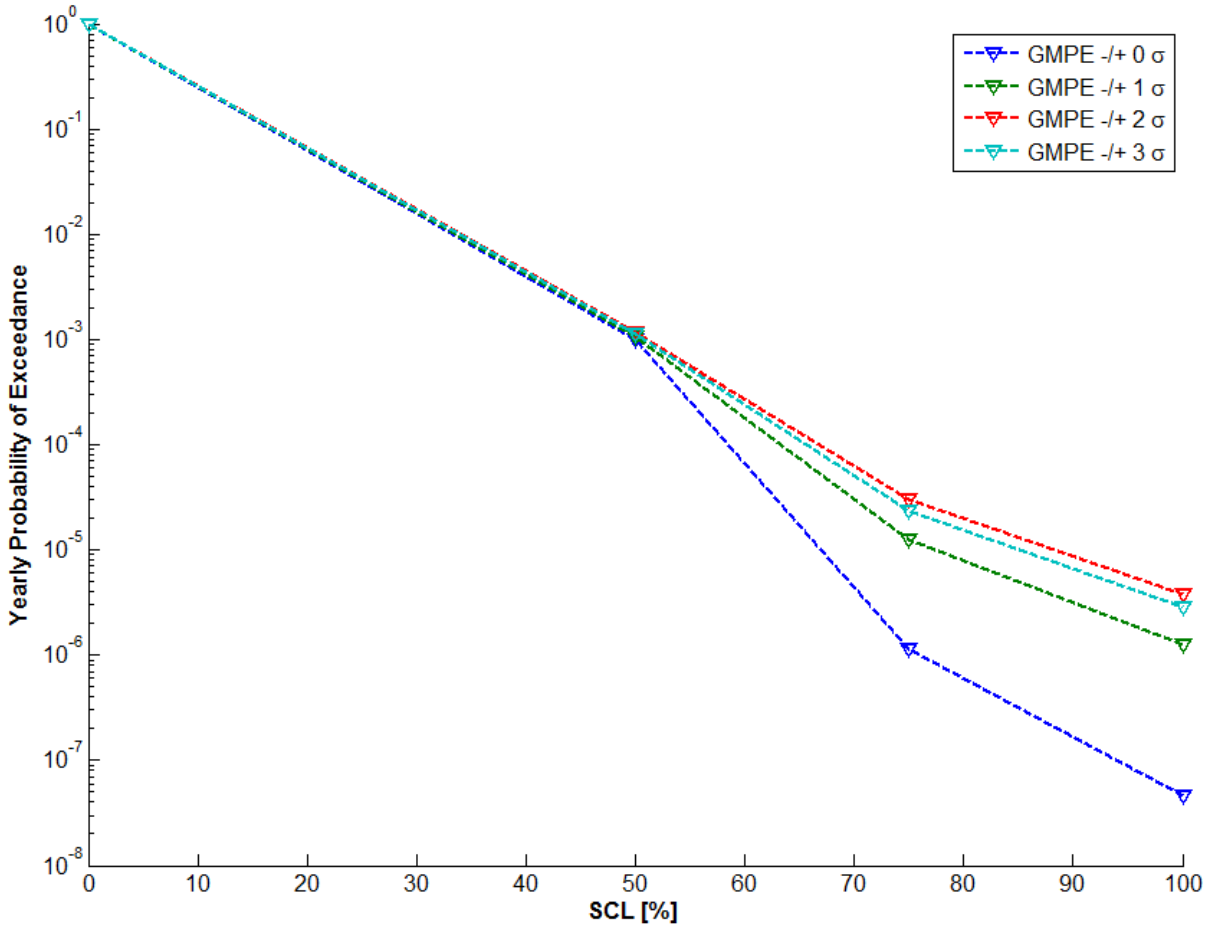

Figure 14: Risk curves for the SCL index, with different assumptions on the aleatory uncertainties associated with the GMPE model

Another variable that is related to the GMPE aleatory uncertainties is the correlation distance of the ground motion field, which is used to express the spatial correlation of the intra-event variability. In the present study, a correlation distance of 13.5 km for PGA has been assumed, based on the recommendations of Akkar and Bommer (2010). The effect of other assumptions (i.e. no spatial correlation or infinite correlation distance) on the global loss of the infrastructure system is represented in Figure 15. It can be observed that the removal of the spatial correlation factor will lead to an underestimation of the risk. This phenomenon may be explained by the definition of the system performance indicator that has been selected. The single connectivity loss SCL counts the number of sources that are still connected to a given sink, while the topology of the present virtual network generates multiple MLSs between each couple of source and sink. Therefore the studied example may be assimilated to a “parallel” system, where multiple paths need to be disrupted for a source to be disconnected and the SCL value to change. Finally, the present problem with a correlation distance of 13.5 km may be adequately bounded by the two extreme assumptions, i.e. no correlation (lower bound) and full correlation (upper bound).

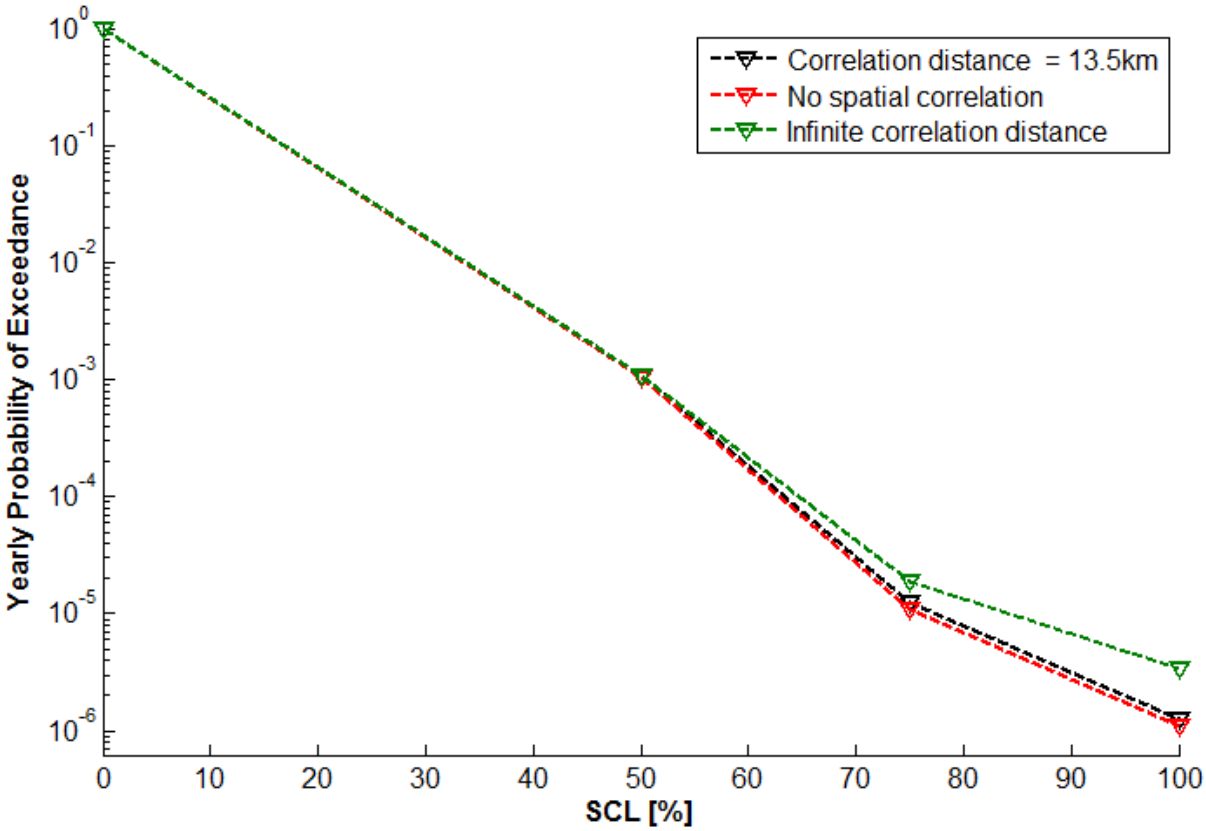

Figure 15: Risk curves for the SCL index, with different assumptions on the spatial correlation distance

Regarding epistemic uncertainties, the variability that is linked to the choice of ground motion model (i.e. GMPE node), to the choice of the seismic fragility curve for bridge B2 (i.e. FRAG node), to the estimation of the slope yield acceleration (i.e. ky node) and the persistence time window is investigated by successively fixing the different states of the mentioned nodes. The assumptions for each uncertainty sources are summarized in **Table 21**.

Uncertainty source	Median value	Lower bound	Upper bound
GMPE	Median GMPE curve	Lower GMPE curve	Upper GMPE curve
FRAG	Median fragility curve	Lower fragility curve	Upper fragility curve
ky	Median ky values from Table 14	Lower ky values from Table 14	Upper ky values from Table 14
ΔT_p	1 month	1 week	3 months

Table 21: Assumptions used for the epistemic uncertainty sources.

The effect of these epistemic uncertainty sources is represented in Figure 16: the largest change is observed when epistemic uncertainties on the ground motion model are considered, however it is much smaller than the discrepancies generated by the aleatory uncertainties (see Figure 14). On the other hand, epistemic uncertainties associated with the FRAG and ky nodes have a very limited impact on the final losses: this may be due mostly to the fact that they are only feeding into a small portion of the infrastructure system (bridge B2 and road along slope, respectively). Finally, the temporal effect, i.e. the change in the value of the persistence time window, is not visible at this

level, even though it has been shown that it has a major impact on the risk bias measure (see **Table 20**). Presently, the only interactions at the fragility level that have been taken into account are the detrimental effect of floods on the seismic fragility of the two bridges B1 and B3. Therefore more multi-risk models for more infrastructure component types and more failure modes should be developed in order to better account for these interaction effects.

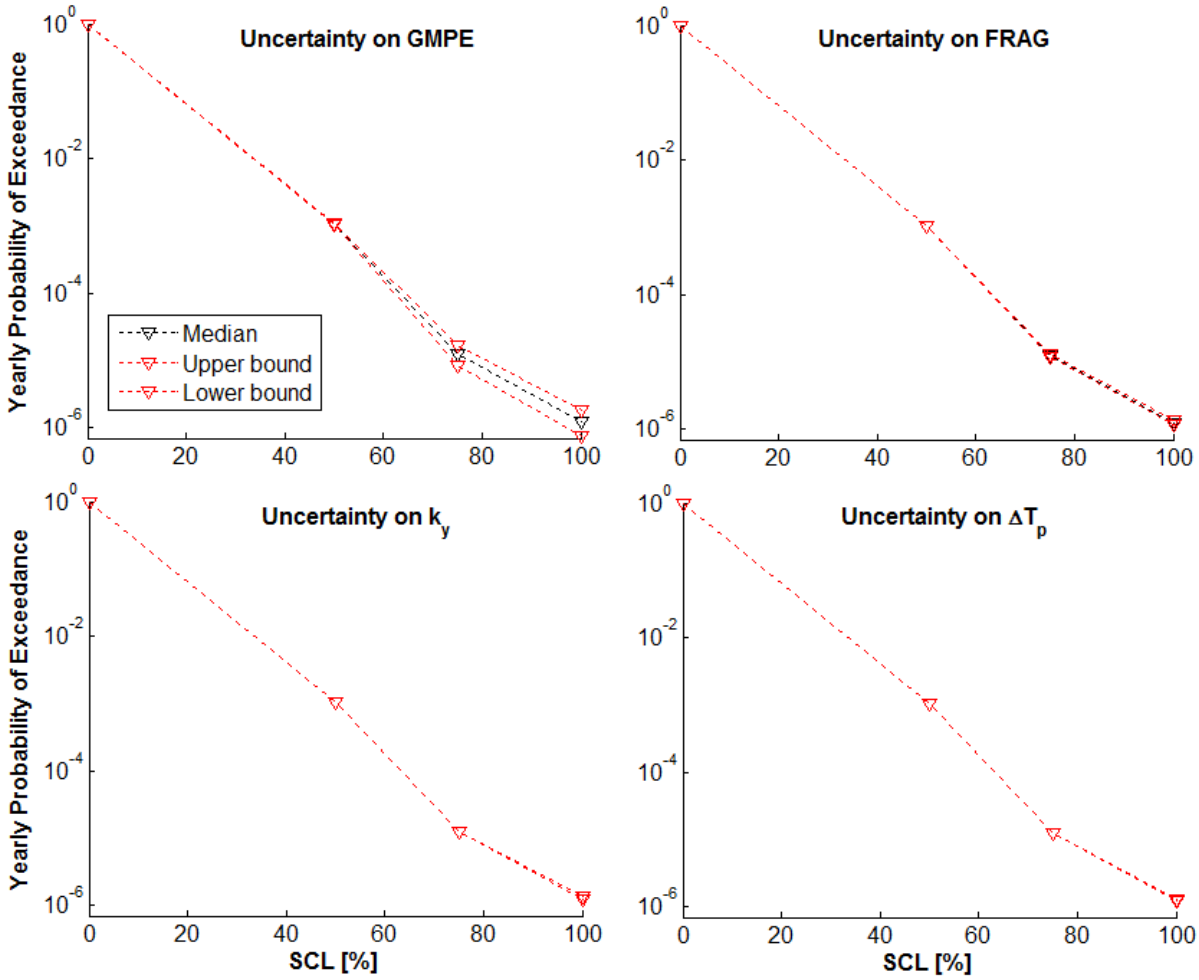

Figure 16: Effect of some sources of epistemic uncertainties on the risk curve

The aggregated effects of the all epistemic uncertainties are summarized in Figure 17, where the upper and lower bounds are defined by taking the worst and best assumptions from **Table 21**, respectively. The epistemic uncertainties are mostly concentrated at the higher loss levels, where a factor of 3 is observed between the probabilities of the upper and lower bounds at SCL=100% (i.e. $2.04.10^{-6}$ vs $6.90.10^{-7}$). However, the present results should come with a significant caveat, since only seismic risk assessment has been the object of uncertainty quantification. The development of a proper assessment method for the flood hazard along with the corresponding uncertainties should be carried out in order to accurately quantify the uncertainty sources that are brought by the different hazard types.

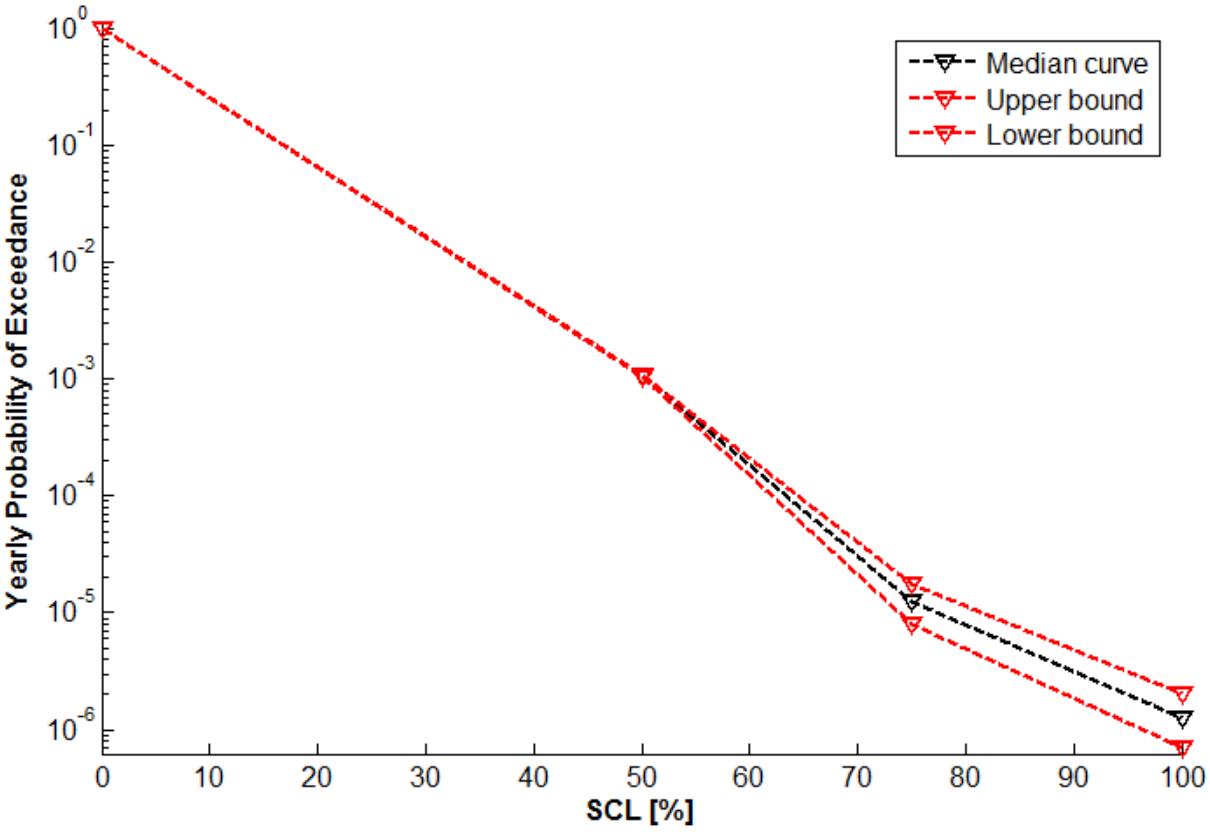

Figure 17: Effect of all considered sources of epistemic uncertainties on the risk curve

4.0 CONCLUSION

Deliverable 3.3 has detailed the various sources of uncertainty that are involved in the risk assessment process for the different hazard types considered in the INFRARISK project (i.e. floods, earthquakes and ground failures). The distinction between aleatory and epistemic uncertainties allows the identification of parameters or which models require further research effort in order to improve the accuracy of the global loss distribution.

The adoption of a Bayesian Network model through a virtual, yet realistic, proof-of-concept example has led to a twofold result:

- The use of an exact inference algorithm provides access to an exact loss distribution, even in the case of extreme events, as opposed to Monte Carlo simulation schemes. Thanks to this feature, the effect of various sources of uncertainties can be quantified, by adding an evidence on the Bayesian nodes of interest and observing the updated loss distributions.
- The Bayesian Network presented here has been used to study multi-risk interactions at both hazard and fragility levels, thanks to the risk decomposition proposed by Selva (2013). By changing the evidences in the BN (e.g. absence or not of the flood or earthquake events, change of the occurrence rate of the earthquake events, etc.), the different risk factors such as single risk, co-active risk, virtual risk and isolated risk, can be easily quantified by using the Bayesian inference.

The study of the effect of the different uncertainty sources has revealed that aleatory uncertainties due to the evaluation of the seismic hazard play an important part in the global risk assessment. Especially, the spatial correlation of the intra-event variability is an essential component of the analysis when considering a distributed system of interdependent components. It has been shown that the global risk may be underestimated when omitting this spatial dependency. Regarding epistemic uncertainties, their combined effect has also been found to be significant, especially for low probability high consequence events, even though additional uncertainty sources should be accounted for when performing a proper flood hazard assessment.

The use of the persistence time window ΔT_p is critical in order to account for the risk interaction between floods and earthquakes. These two hazard events are independent; however it is possible to account for their joint occurrence within a given timeframe that would see flood-damaged components being exposed to potential earthquakes. This time window has a huge effect on the risk bias measure, which identifies the discrepancies between a multi-risk analysis with interactions and superimposed single risk analyses. A bias in the order of 0.5%-1% has been estimated in the present study, which may seem quite modest, especially when comparing with all the other uncertainty sources involved. However, it should be noted that only three components in the considered infrastructure system account for flood-earthquake interactions (i.e. the two bridges B1 and B3, and the road segment exposed to slope failure). Further development of more interactions models would then lead to a higher contribution from multi-risk interactions.

Finally, this work represents the conclusion of the INFRARISK Work Package 3, where all previous tasks and deliverables have been assembled in order to come up with the example of a multi-risk analysis (D3.1 for the hazard assessment, D3.2 for the fragility assessment and D3.4 for the single

risk assessment). Its outcome will feed the different models and input assumptions that will be used in the Integrated Decision Support Tool (IDST) in Work Package 7.

5.0 REFERENCES

Abrahamson, N.A., and Bommer, J.J. (2005). Probability and Uncertainty in Seismic Hazard Analysis, *Earthquake Spectra* 21(2):603-607.

Akkar, S., and Bommer, J.J. (2010). Empirical equations for the prediction of PGA, PGV and spectral accelerations in Europe, the Mediterranean region and the Middle East, *Seismological Research Letters* 81(2):195–206.

Akkar, S., Sandikkaya, M.A., and Bommer, J.J. (2014a). Empirical ground-motion models for point- and extended-source crustal earthquake scenarios in Europe and the Middle East, *Bulletin of Earthquake Engineering* 12(1):359–387.

Akkar, S., Sandikkaya, M.A., Senyurt, M., Azari, S.A., and Ay, B.Ö., Traversa, P., Douglas, J., Cotton, F., Luzi, L., Hernandez, B., and Godey, S. (2014b). Reference database for seismic ground-motion in Europe (RESORCE), *Bulletin of Earthquake Engineering* 12(1):311-339.

Argyroudis, S., and Kaynia, A.M. (2015). Analytical seismic fragility functions for highway and railway embankments and cuts, *Earthquake Engineering and Structural Dynamics*, In press.

Argyroudis, S., Selva, J., Gehl, P., and Pitilakis, K. (2015). Systemic Seismic Risk Assessment of Road Networks Considering Interactions with the Built Environment, *Computer-Aided Civil and Infrastructure Engineering*, In Press.

Atkinson, G.M., and Adams, J. (2013). Ground Motion Prediction Equations for Application to the 2015 Canadian National Seismic Hazard Maps, *Canadian Journal of Civil Engineering* 40(10):988-998.

Bensi, M.T., Der Kiureghian, A., and Straub, D. (2013). Efficient Bayesian Network modelling of systems, *Reliability Engineering and System Safety* 12:200-213.

Bensi, M.T., Der Kiureghian, A., and Straub, D. (2011). A Bayesian Network methodology for infrastructure seismic risk assessment and decision support, PEER Report 2011/02, Pacific Earthquake Engineering Research Center, Berkeley, CA.

Bindi, D., Massa, M., Luzi, L., Ameri, G., Pacor, F., Puglia, R., and Augliera, P. (2014). Pan-European ground-motion prediction equations for the average horizontal component of PGA, PGV, and 5%-damped PSA at spectral periods up to 3.0s using the RESORCE dataset, *Bulletin of Earthquake Engineering* 12(1):391–430.

Bora, S.S., Scherbaum, F., Kuehn, N., and Stafford, P. (2014). Fourier spectral- and duration models for the generation of response spectra adjustable to different source-, propagation-, and site conditions, *Bulletin of Earthquake Engineering* 12(1):467–493.

Bray, J.D., and Travasarou, F. (2007). Simplified procedure for estimating earthquake-induced deviatoric slope displacements, *Journal of Geotechnical and Geoenviromental Engineering,* 133(4):381-392.

Cavalieri, F., Franchin, P., Gehl, P., and Khazai, B. (2012). Quantitative assessment of social losses based on physical damage and interaction with infrastructural systems, *Earthquake Engineering & Structural Dynamics* 41(11):1569-1589.

CDMG (1998), Seismic hazard zone report for the Mint Canyon 7.5-Minute Quadrangle, Los Angeles County, California, California Division of Mines and Geology report, available at http://gmw.consrv.ca.gov/shmp/download/evalrpt/mintc_eval.pdf.

D'Ayala, D., and Gehl, P. (2015). Single Risk Analysis, INFRARISK Technical Report D3.4.

D'Ayala, D., Gehl, P., Martinovic, K., Gavin, K., Clarke, J., Corbally, R., Tucker, M., Avdeeva, Y.V., van Gelder, P., Salceda Page, M.T., and Segarra-Martinez, M.J. (2015). Fragility Functions Matrix, INFRARISK Technical Report D3.2.

D'Ayala, D., Gehl, P., Garcia-Fernandez, M., Jimenez, M.J., Ni Choine, M., Tucker, M., Gavin, K., Martinovic, K., Avdeeva, Y.V., van Gelder, P., Salceda Page, M.T., and Segarra-Martinez, M.J. (2014). Hazard Distribution Matrix, INFRARISK Technical Report D3.1.

Delavaud, E., Cotton, F., Beauval, C., Akkar, S., Scherbaum, F., and Danciu, L. (2012). Construction of a ground-motion logic tree for PSHA in Europe within the SHARE project. Proceedings of the 12th World Conference on Earthquake Engineering, Lisbon, Portugal.

Derras, B., Bard, P.Y., and Cotton, F. (2014). Towards fully data driven ground-motion prediction models for Europe, *Bulletin of Earthquake Engineering* 12(1):495-516.

Douglas, J. (2014). Ground Motion Prediction Equations 1964-2014, Website: www.gmpe.org.uk.

Dunnett, C.W., and Sobel, M. (1955). Approximations to the probability integral and certain percentage points of a multivariate analogue of Student's t-distribution, *Biometrica* 42(1-2):258-260.

Ferrer, F. J. (1993). Recomendaciones para el cálculo hidrometeorológico de avenidas, Madrid, CEDEX, Ministerio de Fomento, 76pp.

Franchin, P. (2014). A Computational Framework for Systemic Seismic Risk Analysis of Civil Infrastructural Systems, In: SYNER-G: Systemic Seismic Vulnerability and Risk Assessment of Complex Urban, Utility, Lifeline Systems and Critical Facilities, K. Pitilakis, P. Franchin, B. Khazai, H. Wenzel (Eds), Springer Netherlands, p23-56.

Franchin, P., and Laura, L. (2014). Probabilistic inference in the physical simulation of interdependent critical infrastructure systems. Proceedings of the SAFECOMP 2014 Workshops, Florence, Italy.

Gehl, P., and D'Ayala, D. (2015a). Integrated multi-hazard framework for the fragility analysis of roadway bridges, Proceedings of the 12th International Conference on Applied Statistics and Probability in Civil Engineering, Vancouver, Canada.

Gehl, P., and D'Ayala, D (2015b). Development of Bayesian Networks for the multi-risk fragility assessment of bridge systems, *Structural Safety*, Under review.

Gehl, P., Ulrich, T., Rohmer, J., Negulescu, C., Ducellier, A., and Douglas, J. (2013). Ranking of epistemic uncertainties in scenario-based seismic risk evaluations. Proceedings of the 11th International Conference on Structural Safety & Reliability, New-York.

Jibson, R.W., Harp, E.L., and Michael, J.A. (2000). A Method for Producing Digital Probabilistic Seismic Landslide Hazard Maps, *Engineering Geology* 58:271–289.

Kameshwar, S., and Padgett, J.E. (2014). Multi-hazard risk assessment of highway bridges subjected to earthquake and hurricane hazards, *Engineering Structures* 78:154-166.

Kjærulff, U. (1990). Triangulation of graphs--algorithms giving small total state space, Institute for Electronic Systems, Aalborg, Denmark.

Marzocchi, W., Sandri, L., and Selva, J. (2010). BET_VH: a probabilistic tool for long-term volcanic hazard assessment, *Bulletin of Volcanology* 72, doi: 10.1007/s00445-010-357-8.

Marzocchi, W., Sandri, L., Gasparini, P., Newhall, C., and Boschi, E. (2004). Quantifying probabilities of volcanic events: The example of volcanic hazard at Mount Vesuvius, *J. Geophys. Res.* 109, doi: 10.1029/2004JB003155.

Mignan, A., Wiemer, S., and Giardini, D. (2014). The quantification of low-probability high-consequence events: part I. A generic multi-risk approach, *Natural Hazards* 73(3):1999-2022.

Murphy, K. (2007). Bayes Net Toolbox, Available from: https://github.com/bayesnet/bnt.

Nielson, B.G. (2005). Analytical fragility curves for highway bridges in moderate seismic zones, PhD Thesis, Georgia Institute of Technology, Georgia.

Pearl, J.G. (1988). Probabilistic reasoning: networks of plausible inference, Morgan Kaufmann, San Francisco, CA.

Poljanšek, K., Bono, F., and Gutiérrez, E. (2012). Seismic risk assessment of interdependent critical infrastructure systems: The case of European gas and electricity networks. *Earthquake Engineering and Structural Dynamics* 41(1):61-79.

Rohmer, J. (2013). Uncertainty quantification: Report on uncertainty quantification and comparison for single-type risk analyses, MATRIX Technical Report D2.2.

Rohmer, J., Douglas, J., Bertil, D., Monfort, D., and Sedan, O. (2014). Weighing the importance of model uncertainty against parameter uncertainty in earthquake loss assessments, *Soil Dynamics and Earthquake Engineering* 58:1-9.

Saygili, G. (2008). A Probabilistic Approach for Evaluating Earthquake-induced Landslides, PhD Thesis, University of Texas, Austin, TX.

Saygili, G., and Rathje, E.M. (2009). Probabilistically based seismic landslide hazard maps: An application in Southern California, *Engineering Geology* 109(3-4):183-194.

Selva, J. (2013). Long-term multi-risk assessment: statistical treatment of interaction among risks, *Natural Hazards* 67:701-722.

Temez, J.R. (1991). Extended and improved rational method, Version of the Highways Administration of Spain, Madrid, Proceedings of XXIV IAHR Congress, 33-40.

van Erp, H.R.N, Linger, R.O., and van Gelder, P.H.A.J.M. (2015). Stress test framework for systems, INFRARISK Technical Report D6.2.

Wen ,W. (1990). Optimal decomposition of belief networks, Proceedings of the 6th Conference on Uncertainty in Artificial Intelligence, Melbourne, Australia.